1. Reply to Editor's comments:

Thank you very much for your valuable comments and suggestions. We have added citation and short discussion of the study of Li et al.(2014) in the revised version, and compared our results with theirs. Answers were shown below.

Editor's Comments: Dear authors
I appreciate the efforts to improve the manuscript. I would say everything is ok, except that I suggest to include citation and short discussion of the most recent addition to the HONO debate based on a measurement campaign in Europe (Li et al., 2014; comment and response). The authors might check whether the consequences for HO_x and RO_x derived for China are comparable to these measurements.

Li, X., Rohrer, F., Hofzumahaus, A., Brauers, T., Häseler, R., Bohn, B., Broch, S., Fuchs, H., Gomm, S., Holland, F., Jäger, J., Kaiser, J., Keutsch, F. N., Lohse, I., Lu, K., Tillmann, R., Wegener, R., Wolfe, G. M., Mentel, T. F., Kiendler-Scharr, A., and Wahner, A.: Missing Gas-Phase Source of HONO Inferred from Zeppelin Measurements in the Troposphere, Science, 344, 292-296, 2014.

Ye, C., Zhou, X., Pu, D., Stutz, J., Festa, J., Spolaor, M., Cantrell, C., Mauldin, R. L., Weinheimer, A., and Haggerty, J.: Comment on "Missing gas-phase source of HONO inferred from Zeppelin measurements in the troposphere", Science, 348, 1326, 2015.

Li, X., Rohrer, F., Hofzumahaus, A., Brauers, T., Häseler, R., Bohn, B., Broch, S., Fuchs, H., Gomm, S., Holland, F., Jäger, J., Kaiser, J., Keutsch, F. N., Lohse, I., Lu, K., Tillmann, R., Wegener, R., Wolfe, G. M., Mentel, T. F., Kiendler-Scharr, A., and Wahner, A.: Response to Comment on "Missing gas-phase source of HONO inferred from Zeppelin measurements in the troposphere", Science, 348, 1326, 2015.

i. Li et al. (2014) suggested that high HONO mixing ratios in the residual layer (RL) in the studied Po Valley in Italy were mainly from a gas-phase source (S_{HONO}) that consumed NO_x, and S_{HONO} was proportional to the photolysis frequency of HONO [J(HONO)], basically consistent with our result that the $P_{unknown}$ was proportional to NO_2 mixing ratios and the photolysis frequency of NO_2 [J(NO_2)].

ii. Table R1 shows the comparison of the calculated S_{HONO} values based on the formula $S_{HONO} = 4.05 \times 10^5 \cdot (ppt \cdot s \cdot h^{-1}) \cdot J(HONO)$ proposed by Li et al. (2014) and the calculated $P_{unknown}$ values based on the formula $P_{unknown} \approx 19.60[NO_2] \cdot J(NO_2)$ in our study. Around noon (10:30 and 10:45 in Table R1), their calculated S_{HONO} values were 2~3 times our calculated $P_{unknown}$ values; in the early morning (before 10:00), the calculated S_{HONO} values by Li et al. (2014) were 5~15 times our $P_{unknown}$ values. The large discrepancy between the $P_{unknown}$ and S_{HONO} values exists due mainly to different meteorological conditions in the early morning and around noon, and different measurements in the RL and near the ground. As stated in the supplement, the $P_{unknown}$ formula was obtained by using the observed data around noon, but Li et al. (2014) used most measurements in early mornings to obtain the S_{HONO} formula. This is also the reason why the mentioned discrepancy above was reduced as the time approached noon. All field experiment data used in our study are near the ground, but the measurements of Li et al. (2014) are in the RL. This difference suggests that more vertical observations of HONO and related other chemical species are needed.

iii. The maximum values of the net OH production rate via the photolysis of HONO subtracting the corresponding reverse reaction, the OH production rate via the reaction of HO_2 + NO, and the OH loss rate via the reaction of OH + NO were within the ranges of our calculations (Table R2).

iv. Li et al. (2014) proposed an assumed HONO source through the reaction between NO_2 and the hydroperoxyl-water complex ($HO_2 \cdot H_2O$), and suggested that the impact of HONO on hydrogen oxide radicals (HO_x) budget could be overestimated because this source mechanism consumed HO_x radicals. However, Ye et al. (2015) argued that the HONO yield for the reaction above is too small (with an upper-limit yield of 0.03) to explain the observation of

HONO in the study of Li et al. (2014), and Li et al. (2015) agreed that the reaction of HO_2 ⇌ H_2O + NO_2 is not a significant HONO source, suggesting that HONO remains an important net OH precursor, as demonstrated by many field studies (e.g., Kleffmann et al., 2005; Acker et al., 2006) and our simulations.

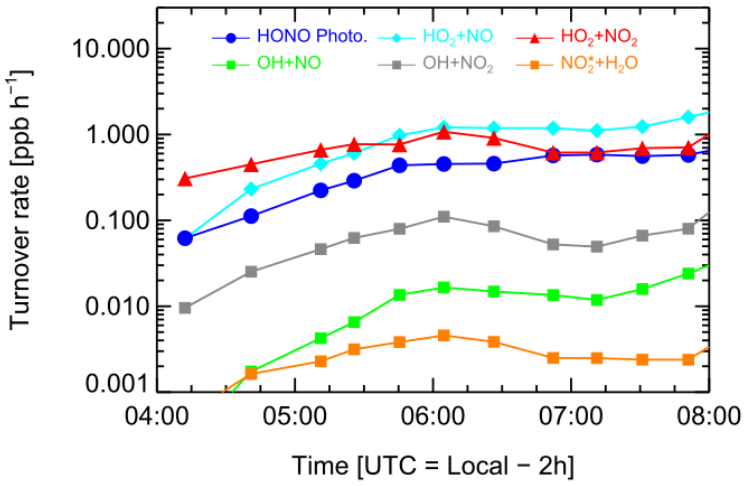

Figure S12: Measured HONO destruction rate, and turnover rates of $HO_2 + NO$, $HO_2 + NO_2$, $OH + NO$, $OH + NO_2$, and $NO_2^* + H_2O$ (*18*) reactions in the residual layer on July 12, 2012 at San Pietro Capofiume, Italy. HO_2 is taken from the model base case scenario M0. All other species were taken from observations.

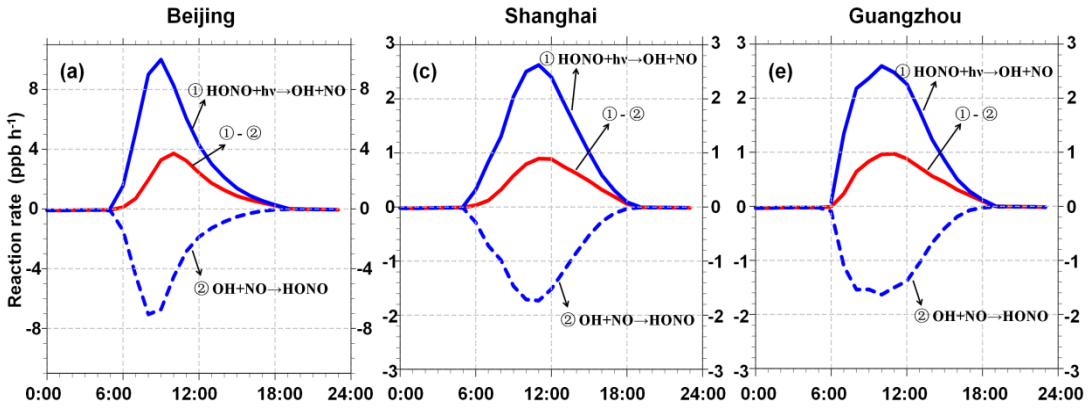

Fig. R1 Averaged reaction rates of HONO+hv→OH+NO（①）, and OH+NO→HONO（②）, and the net OH production rate by HONO photolysis (①-②) for case R_p in (a) Beijing, (b) Shanghai, and (c) Guangzhou in August 2007.

Table R1. Comparison of the calculated HONO source strength (S_{HONO}) based on the formula $S_{HONO} = 4.05\times10^{5}\cdot(ppt\cdot s\cdot h^{-1})\cdot J(HONO)$ proposed by Li et al. (2014) and the calculated $P_{unknown}$ values based on the formula $P_{unknown}\approx 19.60[NO_2]\cdot J(NO_2)$ in our study. The observations of NO_2 mixing ratios ([NO_2]), photolysis frequency of HONO [J(HONO)] were from the measurements by Li et al. (2014). The photolysis frequency of NO_2 [$J(NO_2)$] was calculated from the corresponding measurement of J(HONO) [$J(NO_2) = 5.3\ J(HONO)$] (Kraus and Hofzumahaus, 1998).

Local time	[NO_2] (ppb)	J(HONO) (10^{-3} s^{-1})	$J(NO_2)$ (10^{-3} s^{-1})	S_{HONO} (ppb h^{-1})	$P_{unknown}$ (ppb h^{-1})
6:10	0.7355	0.1114	0.5906	0.0419	0.0085
6:40	0.8667	0.2655	1.4073	0.1128	0.0239
7:10	0.5885	0.5284	2.8005	0.2122	0.0323
7:25	0.6757	0.6380	3.3817	0.2689	0.0448
7:45	0.6338	0.8133	4.3104	0.3329	0.0535
8:05	0.6351	0.9667	5.1237	0.3967	0.0638
8:27	0.4857	1.1421	6.0532	0.4676	0.0576
8:53	0.2934	1.2960	6.8686	0.5242	0.0395
9:12	0.2731	1.4059	7.4514	0.5666	0.0399
9:30	0.2528	1.4725	7.8040	0.5877	0.0387
9:52	0.2541	1.5390	8.1567	0.6230	0.0406
10:12	0.5572	1.6055	8.5094	0.6439	0.0929
10:30	1.3558	1.6502	8.7460	0.6578	0.2324
10:45	1.7878	1.6946	8.9815	0.6718	0.3147

Table R2. Comparison of OH production and loss rates calculated by Li et al. (2014) (Figure S12) and Tang et al. (2015) (Fig. R1 and Table 4).

OH production and loss rates	Li et al. (2014)	Our results
$P_{HONO+hv}$-P_{OH+NO}	0.06~0.57 ppb h^{-1}	0.02~3.86 ppb h^{-1}
P_{OH+NO}	0.002~0.03 ppb h^{-1}	0.03~7.02 ppb h^{-1}
P_{HO2+NO}	0.06~1.56 ppb h^{-1}	1.40~7.10 ppb h^{-1}

References

Acker, K., Möller, D., Wieprecht, W., Meixner, F. X., Bohn, B., Gilge, S., Plass-Dülmer, C., and Berresheim, H.: Strong daytime production of OH from HNO_2 at a rural mountain site, Geophys. Res. Lett., 33(2), doi: 10.1029/2005GL024643, 2006.

Kleffmann, J., Gavriloaiei, T., Hofzumahaus, A., Holland, F., Koppmann, R., Rupp, L., Schlosser, E., Siese, M., Wahner, A.: Daytime formation of nitrous acid: A major source of OH radicals in a forest. Geophysical Research Letters, 32(5), 2005.

Kraus, A., Hofzumahaus, A.: Field measurements of atmospheric photolysis frequencies for O_3, NO_2, HCHO, CH_3CHO, H_2O_2, and HONO by UV spectroradiometry. J. Atmos. Chem., 31: 161-180, 1998.

2. The list of all relevant changes made in the revised manuscript below

A. Change for "2.2 Parameterization of HONO sources"

1) Lines 233-238

B. Changes for "3.4 $P_{unknown}$ impacts on the budgets of OH, HO_2 and RO_2"

1) Lines 421-430

C. Changes for "References"

1) Lines 655-665

2) Lines 795-798

3. The marked-up manuscript version (Changes are in red font)

Impacts of an unknown daytime HONO source on the mixing ratio and budget of HONO, and hydroxyl, hydroperoxyl and organic peroxy radicals, in the coastal regions of China

Yujia Tang[1,2], Junling An[1*], Feng Wang[1,2,3], Ying Li[1], Yu Qu[1], Yong Chen[1], Jian Lin[1,2]

[1]State Key Laboratory of Atmospheric Boundary Layer Physics and Atmospheric Chemistry (LAPC), Institute of Atmospheric Physics (IAP), Chinese Academy of Sciences, Beijing 100029, China

[2]University of the Chinese Academy of Sciences, Beijing 100049, China

[3]Anhui Meteorological Bureau, Hefei 230061, China

[*]Corresponding author: anjl@mail.iap.ac.cn

Abstract

Many field experiments have found high nitrous acid (HONO) mixing ratios in both urban and rural areas during daytime, but these high daytime HONO mixing ratios cannot be explained well by gas-phase production, HONO emissions, and nighttime hydrolysis conversion of nitrogen dioxide (NO_2) on aerosols, suggesting that an unknown daytime HONO source ($P_{unknown}$) could exist. The formula $P_{unknown} \approx 19.60[NO_2] \cdot J(NO_2)$ was obtained using observed data from 13 field experiments across the globe. The three additional HONO sources (i.e., the $P_{unknown}$, nighttime hydrolysis conversion of NO_2 on aerosols, and HONO emissions) were coupled into the WRF-Chem model (Weather Research and Forecasting model coupled with Chemistry) to assess the $P_{unknown}$ impacts on the concentrations and budgets of HONO and peroxy (hydroxyl, hydroperoxyl, and organic peroxy) radicals

(RO_x) (= OH + HO_2 + RO_2) in the coastal regions of China. Results indicated that the additional HONO sources produced a significant improvement in HONO and OH simulations, particularly in the daytime. High daytime average $P_{unknown}$ values were found in the coastal regions of China, with a maximum of 2.5 ppb h^{-1} in the Beijing–Tianjin–Hebei region. The $P_{unknown}$ produced a 60%–250% increase of OH, HO_2 and RO_2 near the ground in the major cities of the coastal regions of China, and a 5%–48% increase of OH, HO_2 and RO_2 in the daytime meridional-mean mixing ratios within 1000 m above the ground. When the three additional HONO sources were included, the photolysis of HONO was the second most important source in the OH production rate in Beijing, Shanghai and Guangzhou before 10:00 LST with a maximum of 3.72 ppb h^{-1} and a corresponding $P_{unknown}$ contribution of 3.06 ppb h^{-1} in Beijing, whereas the reaction of HO_2 + NO (nitric oxide) was dominant after 10:00 LST with a maximum of 9.38 ppb h^{-1} and a corresponding $P_{unknown}$ contribution of 7.23 ppb h^{-1} in Beijing. The whole RO_x cycle was accelerated by the three additional HONO sources, especially the $P_{unknown}$. The daytime average OH production rate was enhanced by 0.67 due to the three additional HONO sources [0.64 due to the $P_{unknown}$] to 4.32 [3.86] ppb h^{-1} via the reaction of HO_2 + NO, and by 0.49 [0.47] to 1.86 [1.86] ppb h^{-1} via the photolysis of HONO, and the OH daytime average loss rate was enhanced by 0.58 [0.55] to 2.03 [1.92] ppb h^{-1} via the reaction of OH + NO_2 and by 0.31 [0.28] to 1.78 [1.64] ppb h^{-1} via the reaction of OH + CO (carbon monoxide) in Beijing, Shanghai and Guangzhou. Similarly, the three additional HONO sources produced an increase of 0.31 [corresponding $P_{unknown}$

contribution of 0.28] to 1.78 [1.64] ppb h^{-1} via the reaction of OH + CO and 0.10 [0.09] to 0.63 [0.59] ppb h^{-1} via the reaction of CH_3O_2 [methylperoxy radical] + NO in the daytime average HO_2 production rate, and 0.67 [0.61] to 4.32 [4.27] ppb h^{-1} via the reaction of HO_2 + NO in the daytime average HO_2 loss rate in Beijing, Shanghai and Guangzhou. The above results suggest that the $P_{unknown}$ considerably enhanced the RO_x concentrations and accelerated RO_x cycles in the coastal regions of China, and could produce significant increases in concentrations of inorganic aerosols and secondary organic aerosols and further aggravate haze events in these regions.

1. Introduction

The hydroxyl radical (OH) is the dominant oxidant in the troposphere, initiating daytime photochemistry, removing the majority of reactive gases, and leading to the formation of secondary products [e.g. ozone (O_3), PANs (peroxyacyl nitrates) and aerosols] that can affect air quality, climate, and human health (Stone et al., 2012). OH is formed primarily through the photolysis of O_3, nitrous acid (HONO), hydrogen peroxide (H_2O_2), the reactions of O_3 with alkenes, and the hydroperoxyl radical (HO_2) to OH conversion process (HO_2+NO) (Platt et al., 1980; Crutzen and Zimmermann, 1991; Atkinson and Aschmann, 1993; Fried et al., 1997; Paulson et al., 1997). Recent field experiments have found that the contribution of the photolysis of HONO to daytime OH production can reach up to 56%, 42% and 33% in urban, rural and forest areas, respectively (Ren et al., 2003; Kleffmann et al., 2005; Acker et

al., 2006), more than that of the photolysis of O_3. However, most current air quality models fail to predict observed HONO concentrations, underestimating daytime HONO in particular (Czader et al., 2012; Gonçalves et al., 2012; Li et al., 2011), due to the incomplete knowledge of HONO sources.

It is generally accepted that the photolysis of HONO [Reaction (R2)] in the early morning could be a major source of OH. After sunrise, HONO mixing ratios are usually in low concentrations due to the strong photolysis of HONO. However, many field experiments have found daytime HONO mixing ratios that are unexpectedly higher than the theoretical steady value (~10 ppt), in both urban and rural areas: e.g., 0.15–1.50 ppb in Asia (Su et al., 2008; Wu et al., 2013; Spataro et al., 2013), 0.01–0.43 ppb in Europe (Kleffmann et al., 2005; Acker et al., 2007; Sörgel et al., 2011; Michoud et al., 2014), 0.02–0.81 ppb in North America (Zhou et al., 2002a,b; Ren et al., 2010; Villena et al., 2011; N. Zhang et al., 2012; Wong et al., 2012; VanderBoer et al., 2013), 2.00 ppb (maximum) in South America (Elshorbany et al., 2009), and 0.015–0.02 ppb in Antarctica (Kerbrat et al., 2012) (Fig. 1). These high HONO mixing ratios, particularly in the daytime, cannot be explained well by gas-phase production [Reaction (R1)], HONO emissions, and nighttime hydrolysis conversion of NO_2 on aerosols, suggesting that an unknown daytime HONO source ($P_{unknown}$) could exist.

$$OH + NO \rightarrow HONO \quad (R1)$$

$$HONO + h\nu \rightarrow OH + NO \quad (R2)$$

$$HONO + OH \rightarrow NO_2 + H_2O \quad (R3)$$

The $P_{unknown}$ was calculated by Su et al. (2008) at Xinken (Guangzhou, China), with a maximum of 4.90 ppb h^{-1}. Spataro et al. (2013) proposed a $P_{unknown}$ value of 2.58 ppb h^{-1} in Beijing. In fact, $P_{unknown}$ values, ranging from 0.06 to 4.90 ppb h^{-1} have been obtained from many field studies across the globe, as shown in Fig. 1, suggesting $P_{unknown}$ could contribute greatly to the daytime production of OH and HO_2.

The most important formation pathway for nocturnal HONO could be the hydrolysis reaction of nitrogen dioxide (NO_2) on humid surfaces [Reaction (R4)] (Kleffmann et al., 1999; Alicke et al., 2002; Finlayson-Pitts et al., 2003):

$$2NO_2 + H_2O \rightarrow HONO + HNO_3 \quad (R4)$$

Ammann et al. (1998) found HONO formation via the heterogeneous reduction of NO_2 on the surface of soot [Reaction (R5)], and Reaction (R5) can be enhanced by irradiation (Monge et al., 2010):

$$NO_2 + red_{ads} \rightarrow HONO + ox_{ads} \quad (R5)$$

George et al. (2005) and Stemmler et al. (2006, 2007) showed the heterogeneous reduction of NO_2 on organic surfaces [Reaction (R6)] (e.g. humic acid) to produce HONO:

$$NO_2 + HC_{red} \rightarrow HONO + HC_{ox} \quad (R6)$$

Li et al. (2008) proposed a homogeneous reaction of photolytically excited NO_2 with H_2O [Reaction (R7)], but this reaction has been proven to be unimportant in the real atmosphere (Carr et al., 2009; Wong et al., 2011; Amedro et al., 2011). Zhang and Tao (2010) suggested the homogeneous nucleation of NO_2, H_2O and ammonia (NH_3)

for the production of HONO [Reaction (R8)], but Reaction (R8) has not yet been tested in laboratory studies, nor observed in field experiments:

$NO_2 + h\upsilon\ (\lambda > 420\ nm) \rightarrow NO_2^*$

$NO_2^* + H_2O \rightarrow HONO + OH$ (R7)

$NO_2^* + M \rightarrow NO_2 + M$

$2NO_2 + H_2O(g) + NH_3 \rightarrow HONO + NH_4NO_3(s)$ (R8)

Zhou et al. (2002b, 2003, 2011) demonstrated that the photolysis of adsorbed nitric acid (HNO_3) and nitrate (NO_3^-) at ultraviolet wavelengths (~300 nm) [Reaction (R9)] can produce HONO:

$HNO_3/NO_3^- + h\upsilon \rightarrow HONO/\ NO_2^- + O$ (R9)

Additionally, HONO could be emitted from soils (Su et al., 2011; Oswald et al., 2013), and may be important in farmland and forest areas.

Based on these mechanisms outlined above, some modeling studies have been carried out to simulate HONO concentrations (e.g. An et al., 2011; Czader et al., 2012; Gonçalves et al., 2012). Sarwar et al. (2008) incorporated Reactions (R4), (R9) and HONO emissions into the Community Multiscale Air Quality (CMAQ) model, but still underestimated HONO mixing ratios during daytime. Li et al. (2010) considered both aerosol and ground surface reactions, and HONO emissions, in the WRF-Chem model (Weather Research and Forecasting model coupled with Chemistry), and found that HONO simulations were significantly improved. However, Li et al. (2010) used a relatively high emissions ratio of 2.3% for $HONO/NO_2$ to compute the direct emissions of HONO, which could have

134 overestimated the HONO concentrations in the air (An et al., 2013). Czader et al.
135 (2012) added Reactions (R6), (R7) and HONO emissions into the CMAQ model.
136 The HONO simulations matched well with observations at night, but were
137 significantly lower than observations at noon. Wong et al. (2013) reported good
138 agreement between simulated and observed daytime HONO when HONO emissions,
139 photolytically enhanced daytime formation mechanisms on both aerosols and the
140 ground, and Reaction (R7), were included. However, according to our recent studies
141 (Tang et al., 2014), this result depended heavily on the selection of uptake
142 coefficients of NO_2 heterogeneous chemistry. Overall, the topic of HONO sources
143 remains under discussion today, and so it is a challenge for modelers to decide which
144 mechanism(s) to be coupled into an air quality model.

145 To investigate the importance of the mechanisms described above, correlation
146 tests between the $P_{unknown}$ and NO_2, HNO_3, irradiation or the photolysis frequency of
147 NO_2 [$J(NO_2)$] were conducted in field experiments (Acker et al., 2007; Sörgel et al.,
148 2011; Villena et al., 2011; Wong et al., 2012). Many of these studies demonstrated
149 that there is a clear dependency of the $P_{unknown}$ on irradiation/$J(NO_2)$ during daytime,
150 particularly at noon. Rohrer et al. (2005) proposed that the photolytic HONO source
151 at the surface of the chamber strongly depended on light intensity. Acker et al. (2007)
152 summarized field experiments in several European countries and showed a strong
153 correlation (R^2=0.81) between the $P_{unknown}$ and $J(NO_2)$. Wong et al. (2012) also
154 indicated that the $P_{unknown}$ showed a clear symmetrical diurnal variation with a
155 maximum around noontime, closely correlated with actinic flux (NO_2 photolysis

156 frequency) and solar irradiance; the correlation coefficient was over 0.70.

157 Besides irradiation/J(NO_2), good correlations between the $P_{unknown}$ and NO_2
158 mixing ratios have been found from both field and laboratory studies, supporting the
159 viewpoint that NO_2 is the primary precursor of HONO. Through estimating the
160 $P_{unknown}$, Acker et al. (2007) speculated that the daytime HONO levels might be
161 explained by a fast electron transfer onto adsorbed NO_2. Sörgel et al. (2011)
162 indicated that the conversion of NO_2 most likely accounted for light-induced HONO
163 formation, about an order of magnitude stronger than HONO formation during
164 nighttime. High correlations between the $P_{unknown}$ and NO_2 mixing ratios have also
165 been found [e.g., R^2 = 0.77 in Qin et al. (2006), R^2 = 0.80 in Villena et al. (2011), and
166 R^2 = 0.62 in Elshorbany et al. (2009)], indicating that the photosensitized conversion
167 of NO_2 is more likely to be the daytime HONO source. This is the reason why the
168 recent CalNex 2010 (California Research at the Nexus of Air Quality and Climate
169 Change) study found a very strong positive correlation (R^2= 0.985) between HONO
170 flux and the product of NO_2 concentration and solar radiation at the Bakersfield site
171 (Ren et al., 2011).

172 Based on the studies introduced above, the $P_{unknown}$ calculated from field
173 experiments may be a practical method to help quantify the daytime HONO source.
174 In this study, field experiment data from 13 different field campaigns across the
175 globe were used to express the $P_{unknown}$ as a function of NO_2 mixing ratios and J(NO_2)
176 (see Sect. 2.2). We then added the $P_{unknown}$ into the WRF-Chem model to assess the
177 impacts of the $P_{unknown}$ on the concentrations and production and loss rates of HONO,

OH, HO_2, and organic peroxy radicals (RO_2).

2. Data and methods

2.1 Observed data

Anthropogenic emissions were based on the year 2006/2007. Limited measurements of HONO, OH, and HO_2 in the coastal regions of China were made in the summers of 2006/2007, so these limited measurements were used for model evaluation. Observed air temperature (TA), relative humidity (RH), wind speed (WS) and direction (WD) near the ground were obtained from the National Climatic Data Center, China Meteorological Administration (H. Zhang et al., 2012). Surface mixing ratios of O_3 and NO_2 in Beijing were obtained from the Beijing Atmospheric Environmental Monitoring Action, carried out by the Chinese Academy of Sciences (Li et al., 2011; Wang et al., 2014), except those in Guangzhou, which were sourced from Qin et al. (2009). HONO observations were conducted using two annular denuders at the campus of Peking University (39°59′N, 116°18′E) in Beijing on 17–20 August 2007 (Spataro et al., 2013) and a long path absorption photometer at the Backgarden (BG) supersite (23°30′N, 113°10′E), about 60 km northwest of Guangzhou on 3–31 July 2006 (X. Li et al., 2012). The measurement systems are described in detail in Spataro et al. (2013) and X. Li et al. (2012). OH and HO_2 were measured by laser induced fluorescence at the BG supersite on 3–30 July 2006 (Lu et al., 2012).

2.2 Parameterization of HONO sources

Besides HONO gas-phase production from Reaction (R1), three additional HONO sources [HONO emissions, Reaction (R4) (nighttime), and the $P_{unknown}$] were coupled into the WRF-Chem model in this work.

HONO emissions were calculated using $[0.023 \times f_{DV} + 0.008 \times (1 - f_{DV})] \times f_{TS}$, where f_{DV} denotes the nitrogen oxides (NO_x) emissions ratio of diesel vehicles to total vehicles, and f_{TS} is the NO_x emissions ratio of the traffic source to all anthropogenic sources (Li et al., 2011; An et al., 2013; Tang et al., 2014). Reaction (R4) was inserted into the Carbon-Bond Mechanism Z (CBM-Z) during nighttime only. The heterogeneous reaction rate was parameterized by $k = \left(\frac{a}{D_g} + \frac{4}{v\gamma} \right)^{-1} A_s$ (Jacob, 2000), where a is the radius of aerosols, v is the mean molecular speed of NO_2, D_g is a gas-phase molecular diffusion coefficient taken as 10^{-5} m^2 s^{-1}(Dentener and Crutzen, 1993), and A_s is the aerosol surface area per unit volume of air, calculated from aerosol mass concentrations and number density in each bin set by the Model for Simulating Aerosol Interactions and Chemistry (MOSAIC). Hygroscopic growth of aerosols was considered (Li et al., 2011).

Previous studies (Sörgel et al., 2010; Villena et al., 2011; Wong et al., 2012) have shown $P_{unknown} \propto [NO_2] \cdot J(NO_2)$. To quantify the relationship between the $P_{unknown}$ and NO_2 mixing ratios and irradiation, daytime $P_{unknown}$, NO_2 mixing ratios and $J(NO_2)$, based on all the available data sets from 13 different field campaigns across the globe (Table S1), were plotted in Fig. 2. As expected, good correlation (R^2 = 0.75) between the $P_{unknown}$ and NO_2 mixing ratios was obtained (Fig. 2a). Furthermore, the correlation between the $P_{unknown}$ and $[NO_2] \cdot J(NO_2)$ was increased

to 0.80, with a linear regression slope of 19.60 (Fig. 2b). For the coastal regions of China (mainly including Laoning, Beijing, Tianjin, Hebei, Shandong, Jiangsu, Anhui, Shanghai, Zhejiang, Jiangxi, Fujian, and Guangdong), the correlation between the $P_{unknown}$ and $[NO_2]\cdot J(NO_2)$ was 0.48, with a linear regression slope of 17.37 (Fig. S2b), which is within the maximum $P_{unknown}$ uncertainty range of 25% (Table S1). The $P_{unknown}$ cloud be expressed as a function of NO_2 mixing ratios and $J(NO_2)$, i.e., $P_{unknown} \approx 19.60[NO_2]\cdot J(NO_2)$. This formula is very similar to $P_{unknown} \approx \alpha \cdot J(NO_2)\cdot[NO_2]\cdot[H_2O]\cdot(S/V_g + S/V_a)$ proposed by Su et al. (2008), and $P_{unknown} \approx 3.3\times10^{-8}[NO_2]\cdot Q_s$ suggested by Wong et al. (2012) as an additional daytime source of HONO through analysis of observed data, where S/V_a is the aerosol surface area-to-volume ratio, S/V_g is the ground surface area-to-volume ratio, α is a fitting parameter, and Q_s is solar visible irradiance. Recently, Li et al. (2014) suggested that high HONO mixing ratios in the residual layer in the studied Po Valley in Italy were mainly from a gas-phase source (S_{HONO}) that consumed NO_x (Li et al., 2015), and S_{HONO} was proportional to the photolysis frequency of HONO [J(HONO)], basically consistent with our result that the $P_{unknown}$ was proportional to NO_2 mixing ratios and the photolysis frequency of NO_2 [$J(NO_2)$].

2.3 Model setup

Used in this study was the WRF-Chem model version 3.2.1 (Grell et al., 2005; Fast et al., 2006), with the CBM-Z (Zaveri and Peters, 1999) and the MOSAIC (Zaveri et al., 2008). The detailed physical and chemical schemes for the simulations can be found in Tang et al. (2014). Two domains with a horizontal resolution of 27 km

were employed in this study: domain 1 covered East Asia, whereas domain 2 covered the coastal regions of China, including the Beijing–Tianjin–Hebei region (BTH), the Yangtze River delta (YRD), and the Pearl River delta (PRD) (Fig. 3), which are the three most rapidly-developing economic growth regions of China. The rapid economic development and urbanization has led to a serious deterioration in air quality in these three regions. Beijing, Shanghai, and Guangzhou are three representative cities of the three regions, so this study focuses on the three regions, including the three representative cities. There were 28 vertical model layers from the ground to 50 hPa, and the first model layer was ~28 m above the ground. Meteorological initial and boundary conditions were obtained from the NCEP (National Centers for Environmental Prediction) $1°\times1°$ reanalysis dataset. Chemical initial and boundary conditions were constrained with the output of MOZART-4 (Model for Ozone and Related chemical Tracers, version 4) (Emmons et al., 2010), every 6 h. Monthly anthropogenic emissions in 2006/2007 and biogenic emissions were the same as those used by Li et al. (2011) and An et al. (2013).

Six simulations (cases R, R_{wop}, and R_p, performed for the entire months of August 2007 and July 2006), with a spin-up period of seven days, were conducted to assess the $P_{unknown}$ effects on the concentrations and budgets of HONO, OH, HO_2, and RO_2. Case R only considered Reaction (R1) as a reference; Case R_{wop} included case R with HONO emissions, and Reaction (R4) only at night; case R_p contained case R_{wop} with the $P_{unknown}$ [$\approx 19.60[NO_2]\cdot J(NO_2)$]. The $P_{unknown}$ and Reaction (R4) were added to the CBM-Z, and diagnostic variables (i.e., production and loss rates of HONO, OH,

HO_2, RO_2, O_3, and other species) were inserted into the CBM-Z to quantify the $P_{unknown}$ impacts on the budgets of HONO, OH, HO_2, and RO_2 (Wang et al., 2014).

3. Results and discussion

3.1 Comparison of simulations and observations

The statistical metrics of mean bias (MB), mean error (ME), root-mean-square error (RMSE), normalized mean bias (NMB), normalized mean error (NME), index of agreement (IOA), and correlation coefficient (CC), were used. The MB, ME, and RMSE are given in the same units as the measurements (absolute metrics). The MB quantifies the tendency of the model to over- or underestimate values, while the ME and RMSE measure the magnitude of the difference between modeled and observed values regardless of whether the modeled values are higher or lower than observations. One disadvantage of absolute metrics is that they make intercomparisons of model performance in clean and polluted environments or across different pollutants difficult to interpret. Consequently, a range of relative metrics are often used. These metrics are presented either in fractional or percentage units. The NMB and NME all normalize by observed values. The IOA and CC provide a sense of the strength of the relationship between model estimates and observations that have been paired in time and space. Perfect agreement for any metric alone may not be indicative of good model performance, so multiple metrics must be considered when evaluating model performance. Simulations of TA, RH, WS and WD were compared with observations, as shown in Wang et al. (2014). The MB, ME, RMSE, NMB, NME, IOA, and CC were comparable with those of Wang

et al. (2010) and L. Li et al. (2012) using MM5 (the fifth-generation Pennsylvania State University/National Center for Atmospheric Research Mesoscale Model), and H. Zhang et al. (2012) using the WRF model. For O_3 in Beijing of the BTH region and Guangzhou of the PRD region, the NMB, NME and IOA were −22.80%, 58.70% and 0.79, respectively (Table 1 for case R), comparable to the values of 30.2% for NMB, 55.8% for NME and 0.91 for IOA reported in L. Li et al. (2012) using the CMAQ model. When HONO emissions, Reaction (R4) and the $P_{unknown}$ were included, the NMB, NME and IOA increased to −2.20%, 66.10% and 0.80, respectively (Table 1 for case R_p). The NO_2 fluctuations were generally captured (Fig. 4) but the simulated amplitude of NO_2 was underestimated in some cases (Fig. 4). This underestimation could be related with the uncertainty of NO_x emissions. For NO_2 in case R, the NMB, NME and IOA were −13.50%, 42.10% and 0.57, respectively (Table 1), similar to the results of Wang et al. (2010) using the CMAQ model (NMB of −33.0%, NME of 50.0%, and IOA of 0.61). Compared with case R, NO_2 simulations (Table 1 for case R_p) were further underestimated for case R_p due to the underestimation of NO_x emissions in Guangzhou.

HONO simulations only with the gas-phase production (case R) were always substantially underestimated compared with observations (Fig. 5), similar to the results of Sarwar et al. (2008), Li et al. (2011) and An et al. (2013). When HONO emissions and Reaction (R4) were included, HONO simulations were significantly improved, especially at night (Fig. 5 and Table 2 for case R_{wop}). For Beijing, the nighttime RMSE and NME were reduced by 0.90×10^6 molecules cm^{-3} and 44.70%,

whereas the NMB and IOA were increased by 50.00% and 0.29, respectively (Table 2). For Guangzhou, the nighttime RMSE and NME were reduced by 0.44 × 10^6 molecules cm^{-3} and 32.90%, and the NMB and IOA were enhanced by 58.80% and 0.18, respectively. When the $P_{unknown}$ was included, daytime HONO simulations were considerably improved (Fig. 5 and Table 2 for case R_p). Compared with case R_{wop}, the daytime NME in Beijing was reduced by 19.60%, and the NMB and IOA in Beijing were increased to −24.30% from −62.00% and 0.73 from 0.64, respectively (Table 2); the daytime NME in Guangzhou was reduced by 8.10%, and the NMB in Guangzhou was increased to −61.20% from −76.50% (Table 2).

Simulated diurnal variations of OH and HO_2 showed consistent patterns with the observed data (Fig. 6). When HONO emissions and Reaction (R4) were considered (case R_{wop}), OH and HO_2 enhancements were ≤ ~6% in most cases compared with case R (Fig. 6 and Table 3), but the $P_{unknown}$ led to 10%–150% improvements in OH simulations on 5–12 July 2006 (Fig. 6). The 20%–90% overestimation of OH mixing ratios on 20–25 July 2006 (Fig. 6) needs further investigation. Compared with case R, the NME was reduced by 79.60% (=136.60% − 57.00%), whereas the NMB was increased by 105.40% (123.00% − 17.60%), and the IOA was improved to 0.84 from 0.79 (Table 3). When the $P_{unknown}$ was considered, HO_2 simulations were substantially improved (Fig. 6), the IOA was improved to 0.61 from 0.54 and the CC was improved to 0.66 from 0.57 (Table 3). However, HO_2 simulations were still substantially underestimated (Fig. 6). One of the major reasons for the HO_2 underestimation could be related to the considerable

underestimation of anthropogenic volatile organic compounds (VOCs) (Wang et al., 2014).

3.2 $P_{unknown}$ simulations and its impacts on production and loss rates of HONO

High $P_{unknown}$ values were found in the coastal regions of China (Fig. 7), especially in the BTH, YRD and PRD regions due to elevated emissions of NO_x (Zhang et al., 2009). The largest daytime average $P_{unknown}$ value reached 2.5 ppb h^{-1} in Tianjin of the BTH region (Fig. 7a), whereas it was 2.0 ppb h^{-1} in Shanghai of the YRD region (Fig. 7b). The largest daytime average $P_{unknown}$ value reached 1.2 ppb h^{-1} in Guangzhou and Shenzhen of the PRD (Fig. 7c), lower than the values of 2.5 ppb h^{-1} and 2.0 ppb h^{-1}. One major reason is the underestimation of daytime NO_2 mixing ratios in the PRD (Fig. 4b).

For case R, daytime HONO production was primarily from the reaction of OH and nitric oxide (NO) [Reaction (R1)], with a maximum production rate of 0.69 ppb h^{-1} in Beijing, 1.20 ppb h^{-1} in Shanghai, and 0.72 ppb h^{-1} in Guangzhou near noon due to high OH mixing ratios (Fig. 8a, c, e). The loss rate of HONO was 0.62 ppb h^{-1} in Beijing, 1.09 ppb h^{-1} in Shanghai, and 0.65 ppb h^{-1} in Guangzhou via Reaction (R2), much higher than the 0.01–0.02 ppb h^{-1} in Beijing, Shanghai and Guangzhou via Reaction (R3) (Fig. 8b, d, f), indicating that Reaction (R2) accounted for approximately 99% of the total loss rate of HONO.

When the additional HONO sources [HONO emissions, Reaction (R4), and the $P_{unknown}$] were coupled into the WRF-Chem model, nighttime HONO was formed mainly via Reaction (R4) (0.30–1.42 ppb h^{-1} in Beijing, 0.20–0.45 ppb h^{-1} in

354 Shanghai, and 0.25–0.84 ppb h^{-1} in Guangzhou) (Fig. 8a, c, e). HONO emissions
355 contributed 0.04–0.62 ppb h^{-1} to HONO production (Fig. 8a, c, e). Simulated
356 $P_{unknown}$ values ranged from 0.42 to 2.98 ppb h^{-1} in Beijing, from 0.18 to 2.58 ppb
357 h^{-1} in Shanghai, and from 0.06 to 1.66 ppb h^{-1} in Guangzhou (Fig. 8a, c, e). The
358 simulated $P_{unknown}$ values in Beijing (Fig. 8a) were in good agreement with the
359 results of Spataro et al. (2013), with an average unknown daytime HONO production
360 rate of 2.58 ppb h^{-1} in the studied summer period. However, the simulated $P_{unknown}$
361 values in Guangzhou (Fig. 8e) were lower than the 2.36–4.90 ppb h^{-1} reported by Su
362 et al (2008), due mainly to the underestimation of the daytime NO_2 mixing ratios in
363 the PRD region. The additional HONO sources produce more HONO, which
364 subsequently photolyzes to yield more OH. Therefore, the formation of HONO
365 through Reaction (R1) was greatly enhanced, with a maximum of 4.70 [1.44 due to
366 the $P_{unknown}$] ppb h^{-1} in Beijing, 4.25 [3.13] ppb h^{-1} in Shanghai, and 1.58 [0.40] ppb
367 h^{-1} in Guangzhou in the morning (Fig. 8a, c, e), much higher than the 0.69 ppb h^{-1} in
368 Beijing, 1.20 ppb h^{-1} in Shanghai, and 0.72 ppb h^{-1} in Guangzhou, respectively, for
369 case R (Fig. 8a, c, e). Meanwhile, the loss rate of HONO via Reaction (R2) was
370 significantly enhanced, with a maximum enhancement of 5.20 (= 5.82 − 0.62) [1.97
371 due to the $P_{unknown}$] ppb h^{-1} in Beijing, 4.31 (= 5.40 − 1.09) [1.44] ppb h^{-1} in
372 Shanghai, and 1.96 (= 2.61 − 0.65) [1.18] ppb h^{-1} in Guangzhou (Fig. 8b, d, f). The
373 HONO loss rate via dry deposition ranged from 0.28 to 0.45 ppb h^{-1} (not shown),
374 roughly equivalent to the contribution of HONO emissions, suggesting that dry
375 deposition of HONO cannot be neglected in high NO_x emission areas. The maximum

$P_{unknown}$ uncertainty range of 25% (Table S1), a 25% increase (decrease) in the slope factor (19.60) led to a 9.19%–18.62% increase (a 8.40%–14.32% decrease) in the maximum production and loss rate of HONO (Fig. S3).

3.3 $P_{unknown}$ impacts on concentrations of OH, HO_2 and RO_2

Incorporation of the $P_{unknown}$ into the WRF-Chem model led to substantial enhancements in the daytime average mixing ratios of OH in the coastal regions of China, e.g., 60%–190% in the BTH region, 60%–210% in the YRD region, and 60%–200% in the PRD region (Fig. 9a). The maximum enhancement of HO_2 reached 250% in the BTH region, 200% in the YRD region, and 140% in the PRD region (Fig. 9b). Similarly, a daytime average increase of 100%–180%, 60%–150% and 40%–80% in RO_2 [= CH_3O_2 (methylperoxy radical) + ETHP (ethylperoxy radical) + C_2O_3 (peroxyacyl radical) + others] were found in the BTH, YRD and PRD regions, respectively (Fig. 9c).

Vertically, the $P_{unknown}$ enhanced the monthly meridional-mean daytime (06:00–18:00 LST) mixing ratios of OH, HO_2 and RO_2 by 5%–38%, 5%–47% and 5%–48%, respectively, within 1000 m above the ground in the coastal regions of China (Fig. 10). Strong vertical mixing in the daytime in summer led to a roughly uniform vertical enhancement of OH, HO_2 and RO_2 within the 1000 m at the same latitude (Fig. 10). Different $P_{unknown}$ values in different latitudes produced distinct differences in the enhancements of OH, HO_2 and RO_2, with a maximum located near 35 ℃N (Fig. 10).

3.4 $P_{unknown}$ impacts on the budgets of OH, HO_2 and RO_2

OH radicals are produced mainly through the reaction of HO_2 + NO, the photolysis of O_3 and HONO, and the reactions between O_3 and alkenes (Fig. 11). For case R, the predominant contribution to P(OH) (production rate of OH) was the reaction of HO_2 + NO (Fig. S1a, c, e), and the photolysis of O_3 was the second most important source of OH (Fig. S1a, c, e). When the three additional HONO sources were added, the most important source was the reaction of HO_2 + NO, with a diurnal maximum conversion rate reaching 9.38 [7.23 due to the $P_{unknown}$] ppb h^{-1} in Beijing, 2.63 [1.15] ppb h^{-1} in Shanghai, and 4.88 [1.43] ppb h^{-1} in Guangzhou near noon (Fig. 11a, c, e). The photolysis of HONO became the second most important source of OH in Beijing and Guangzhou before 10:00 LST, and in Shanghai before 12:00 LST; the diurnal peaks were 3.72 [3.06] ppb h^{-1} in Beijing at 09:00 LST, 0.89 [0.62] ppb h^{-1} in Shanghai at 11:00 LST, and 0.97 [0.78] ppb h^{-1} in Guangzhou at 09:00 LST (Fig. 11a, c, e), which were comparable to or lower than the 3.10 ppb h^{-1} reported by Elshorbany et al. (2009). Kanaya et al. (2009), who also conducted similar studies at Mount Tai (located in a rural area) of China, using an observationally constrained box model, suggested that the reaction of HO_2 + NO was the predominant OH source, with a daytime average of 3.72 ppb h^{-1}, more than the 1.38 ppb h^{-1} of the photolysis of O_3. Using an observationally constrained box model, Hens et al. (2014) reported similar results in a boreal forest, in which the dominant contributor to OH was the reaction of HO_2 + NO, ranging from 0.23 to 1.02 ppb h^{-1} during daytime. The production rates of OH in our study were higher than in Kanaya

et al. (2009) and Hens et al. (2014) due to higher NO_x emissions in urban areas than in rural areas.

Recently, Li et al. (2014) proposed an assumed HONO source through the reaction between NO_2 and the hydroperoxyl-water complex (HO_2 ·H_2O), and suggested that the impact of HONO on hydrogen oxide radicals (HO_x) budget could be overestimated because this source mechanism consumed HO_x radicals. However, Ye et al. (2015) argued that the HONO yield for the reaction above is too small (with an upper-limit yield of 0.03) to explain the observation of HONO in the study of Li et al. (2014), and Li et al. (2015) agreed that the reaction of HO_2 ·H_2O + NO_2 is not a significant HONO source, suggesting that HONO remains an important net OH precursor, as demonstrated by many field studies (e.g., Kleffmann et al., 2005; Acker et al., 2006) and our simulations.

The dominant loss rate of OH was the reaction of OH + NO_2 for both cases R and R_p (Figs. 11b, d, f and S1b, d, f). The diurnal maximum loss rates were 1.98 ppb h^{-1} in Beijing, 1.12 ppb h^{-1} in Shanghai, and 1.70 ppb h^{-1} in Guangzhou for case R (Fig. S1b, d, f), whereas these values were 5.61 [4.38 due to the $P_{unknown}$] ppb h^{-1} in Beijing, 2.00 [1.00] ppb h^{-1} in Shanghai, and 2.65 [1.02] ppb h^{-1} in Guangzhou for case R_p (Fig. 11b, d, f). The reactions of OH + VOCs to form HO_2 and RO_2 were the second most important loss path of OH, with a diurnal maximum of 0.75–1.73 ppb h^{-1} for case R (Fig. S1b, d, f) and 1.57 [0.82 due to the $P_{unknown}$] to 5.37 [4.05] ppb h^{-1} for case R_p in Beijing, Shanghai and Guangzhou (Fig. 11b, d, f). The third most important OH loss path was the reaction of OH + CO to form HO_2; the diurnal

maximum rates were 0.46–1.47 ppb h^{-1} for case R (Fig. S1b, d, f) and 0.93 [0.49 due to the $P_{unknown}$] to 3.58 [2.86] ppb h^{-1} for case R_p in Beijing, Shanghai and Guangzhou (Fig. 11b, d, f).

The averaged radical conversion rates in the daytime (06:00–18:00 LST) are illustrated in Fig. 12. OH radicals are produced mainly via the photolysis of O_3, HONO and hydrogen peroxide (H_2O_2), and the reactions between O_3 and alkenes, after which OH radicals enter the RO_x (= OH + HO_2 + RO_2) cycle (Fig. 12 and Tables 4, S2 and S3).

For case R, the reaction of HO_2 + NO was the major source of OH [2.78 ppb h^{-1} (81.73% of the total daytime average production rate of OH) in Beijing, 0.73 ppb h^{-1} (67.09%) in Shanghai, and 1.75 ppb h^{-1} (71.54%) in Guangzhou] (Fig. 12a and Table 4). The second largest source of OH was the photolysis of O_3 (Table 4). OH radicals were removed mainly through the reaction of OH + NO_2 [1.12 ppb h^{-1} (39.31% of the total daytime average loss rate of OH) in Beijing, 0.47 ppb h^{-1} (46.63%) in Shanghai, and 0.77 ppb h^{-1} (38.33%) in Guangzhou] (Table 4), whereas those were converted to HO_2 mainly via the reaction of OH + CO (Table 4). For HO_2, the predominant production pathways were the reactions of OH + CO and CH_3O_2 + NO and the photolysis of formaldehyde (HCHO) (Table S2). HO_2 radicals were consumed primarily via the reaction of HO_2 + NO [2.78 ppb h^{-1} (99.34%) in Beijing, 0.73 ppb h^{-1} (99.61%) in Shanghai, and 1.75 ppb h^{-1} (98.29%) in Guangzhou] (Table S2). RO_2 radicals were formed mainly from the reactions of OH + OLET (terminal olefin carbons)/OLEI (internal olefin carbons), OH + ETH (ethene), OH + methane

463 (CH_4), and OH + AONE (acetone). RO_2 radicals were consumed primarily via the
464 reaction of CH_3O_2 + NO [0.54 ppb h^{-1} (94.56%) in Beijing, 0.16 ppb h^{-1} (95.28%) in
465 Shanghai, and 0.33 ppb h^{-1} (96.07%) in Guangzhou] (Table S3).

466 When the three additional HONO sources were inserted into the WRF-Chem
467 model (case R_p), the daytime average OH production rate was enhanced by 4.32 (=
468 7.10 − 2.78) [3.86 due to the $P_{unknown}$] ppb h^{-1} in Beijing, 0.67 (= 1.40 − 0.73) [0.64]
469 ppb h^{-1} in Shanghai, and 0.80 (= 2.55 − 1.75) [0.68] ppb h^{-1} in Guangzhou via the
470 reaction of HO_2 + NO, and by 1.86 [1.86] ppb h^{-1} in Beijing, 0.50 [0.50] ppb h^{-1} in
471 Shanghai, and 0.49 [0.47] ppb h^{-1} in Guangzhou via the photolysis of HONO,
472 respectively (Table 4). The enhancements of the daytime average OH production rate
473 due to the photolysis of HONO were comparable to or lower than the 2.20 ppb h^{-1}
474 obtained by Liu et al. (2012). The daytime average OH loss rate was increased by
475 2.03 [1.92 due to the $P_{unknown}$] ppb h^{-1} in Beijing, 0.58 [0.55] ppb h^{-1} in Shanghai,
476 and 0.65 [0.58] ppb h^{-1} in Guangzhou via the reaction of OH + NO_2, and by 1.78
477 [1.64] ppb h^{-1} in Beijing, 0.31 [0.28] ppb h^{-1} in Shanghai, and 0.42 [0.36] ppb h^{-1} in
478 Guangzhou via the reaction of OH + CO, respectively (Table 4). Similarly, the
479 daytime average HO_2 production rate was increased by 0.31 [0.28 due to the $P_{unknown}$]
480 to 1.78 [1.64] ppb h^{-1} in Beijing, Shanghai and Guangzhou via the reaction of OH +
481 CO, and by 0.63 [0.59] ppb h^{-1} in Beijing, 0.10 [0.09] ppb h^{-1} in Shanghai, and 0.19
482 [0.17] ppb h^{-1} in Guangzhou via the reaction of CH_3O_2 + NO; whereas, the daytime
483 average HO_2 loss rate was enhanced by 0.67 [0.61 due to the $P_{unknown}$] to 4.32 [4.27]
484 ppb h^{-1} in Beijing, Shanghai and Guangzhou via the reaction of HO_2 + NO (Table

S2).

Overall, the net daytime production rate of RO_x was increased to 3.48 (= 2.56 + 0.71 + 0.21) [2.06 due to the $P_{unknown}$] from 1.20 (= 0.60 + 0.43 + 0.17) ppb h^{-1} in Beijing, 1.09 (= 0.86 + 0.19 + 0.04) [0.45] from 0.54 (= 0.36 + 0.14 + 0.04) ppb h^{-1} in Shanghai, and 1.52 (= 1.21 + 0.26 + 0.05) [0.58] from 0.92 (= 0.68 + 0.20 + 0.04) ppb h^{-1} in Guangzhou (Fig. 12) due to the three additional HONO sources, indicating that the RO_x source was mainly from OH production, especially via the photolysis of HONO (Tables 4, S2 and S3). This result is different from the conclusion of Liu et al. (2012) that the photolysis of HONO and oxygenated VOCs is the largest RO_x source. One of the primary reasons for this is the underestimation of anthropogenic VOCs (Wang et al., 2014). For Beijing, the net production rate of RO_x was 3.48 ppb h^{-1}, lower than the 6.60 ppb h^{-1} from the field studies of Liu et al. (2012). Our results reconfirmed the view of Ma et al. (2012) that the North China Plain acts as an oxidation pool. The additional HONO sources produced an increase of 2.03 [1.96 due to the $P_{unknown}$] ppb h^{-1} in Beijing, 0.56 [0.54] ppb h^{-1} in Shanghai, and 0.66 [0.59] ppb h^{-1} in Guangzhou in the net loss rate of RO_x (Fig. 12).

4. Conclusions

The relationship between the $P_{unknown}$, NO_2 mixing ratios and $J(NO_2)$ was investigated using available data from 13 field studies across the globe. The formula $P_{unknown} \approx 19.60[NO_2] \cdot J(NO_2)$ was obtained, and then the three additional HONO sources (i.e., the $P_{unknown}$, HONO emissions and nighttime hydrolysis conversion of NO_2 on aerosols) were inserted into the WRF-Chem model, to assess

the $P_{unknown}$ impacts on the concentrations and budgets of HONO and RO_x in the coastal regions of China. The results showed that:

(1) The additional HONO sources led to significant improvements in the simulations of HONO and OH, especially in the daytime.

(2) Elevated daytime average $P_{unknown}$ values were found in the coastal regions of China, reaching 2.5 ppb h^{-1} in the BTH region, 2.0 ppb h^{-1} in the YRD region, and 1.2 ppb h^{-1} in the PRD region.

(3) The additional HONO sources substantially enhanced the production and loss rates of HONO. Dry deposition of HONO contributed 0.28–0.45 ppb h^{-1} to the loss rate of HONO, approximately equivalent to the contribution of HONO emissions, emphasizing the importance of dry deposition of HONO in high NO_x emissions areas.

(4) The $P_{unknown}$ produced a 60%–210% enhancement of OH, a 60%–250% enhancement of HO_2, and a 60%–180% enhancement of RO_2 near the ground in the major cities of the coastal regions of China. Vertically, the $P_{unknown}$ enhanced the daytime meridional-mean mixing ratios of OH, HO_2 and RO_2 by 5%–38%, 5%–47% and 5%–48%, respectively, within 1000 m above the ground.

(5) When the three additional HONO sources were added, the photolysis of HONO became the second most important source of OH in Beijing and Guangzhou before 10:00 LST, and in Shanghai before 12:00 LST, with a maximum of 3.72 [3.06 due to the $P_{unknown}$] ppb h^{-1} in Beijing, 0.89 [0.62] ppb h^{-1} in Shanghai, and 0.97 [0.78] ppb h^{-1} in Guangzhou; whereas, the reaction of HO_2 + NO was the most

important source of OH, dominated in Beijing and Guangzhou after 10:00 LST and in Shanghai after 12:00 LST, with a maximum of 9.38 [7.23] ppb h^{-1} in Beijing, 2.63 [1.15] ppb h^{-1} in Shanghai, and 4.88 [1.43] ppb h^{-1} in Guangzhou.

Overall, the above results suggest that the $P_{unknown}$ significantly enhances the atmospheric oxidation capacity in the coastal regions of China by increasing RO_x concentrations and accelerating RO_x cycles, and could lead to considerable increases in concentrations of inorganic aerosols and secondary organic aerosols and further aggravate haze events in these regions.

Acknowledgements

This research was partially supported by the National Natural Science Foundation of China (41175105, 41405121), a Key Project of the Chinese Academy of Sciences (XDB05030301), and the Carbon and Nitrogen Cycle Project of the Institute of Atmospheric Physics, Chinese Academy of Sciences, and the Beijing Municipal Natural Science Foundation (8144054).

References

Acker, K., Möller, D.: Corrigendum to: Atmospheric variation of nitrous acid at different sites in Europe. Environmental Chemistry, 4(5), 364-364, 2007.

Acker, K., Möller, D., Wieprecht, W., Meixner, F. X., Bohn, B., Gilge, S., Plass-Dülmer, C., and Berresheim, H.: Strong daytime production of OH from HNO_2 at a rural mountain site, Geophys. Res. Lett., 33(2), doi:

10.1029/2005GL024643, 2006.

Alicke, B., Platt, U., and Stutz, J.: Impact of nitrous acid photolysis on the total hydroxyl radical budget during the limitation of oxidant production/Pianura padana produzione di ozono study in Milan, J. Geophys. Res. –Atmos., 107(D22): LOP9-1 – LOP9-17, doi: 10.1029/2000JD000075, 2002.

Amedro, D., Parker, A. E., Schoemaecker, C., Fittschen, C.: Direct observation of OH radicals after 565nm multi-photon excitation of NO_2 in the presence of H_2O. Chemical Physics Letters, 513(1), 12-16, 2011.

Ammann, M., Kalberer, M., Jost, D. T., Tobler, L., Rössler, E., Piguet, D., Gäggeler, H., Baltensperger, U.: Heterogeneous production of nitrous acid on soot in polluted air masses. Nature, 395(6698), 157-160, 1998.

An, J., Li, Y., Wang, F., and Xie, P.: Impacts of photoexcited NO_2 chemistry and heterogeneous reactions on concentrations of O_3 and NO_y in Beijing, Tianjin and Hebei province of China, Air Quality-Models and Applications, Prof. Dragana Popovic (Ed.), InTech, ISBN: 978-953-307-307-1, doi: 10.5772/16858, 2011.

An, J., Li, Y., Chen, Y., Li, J., Qu, Y., Tang, Y.: Enhancements of major aerosol components due to additional HONO sources in the North China Plain and implications for visibility and haze. Advances in Atmospheric Science, 30, 57-66, 2013.

Atkinson, R., Aschmann, S. M.: Hydroxyl radical production from the gas-phase reactions of ozone with a series of alkenes under atmospheric

573 conditions. Environmental science & technology, 27(7), 1357-1363, 1993.
574 Carr, S., Heard, D., Blitz, M.: Comment on "Atmospheric Hydroxyl Radical
575 Production from Electronically Excited NO_2 and H_2O". Science, 324, 5925,
576 doi:10.1126/science.1166669, 2009.
577 Crutzen, P. J., Zimmermann, P. H.: The changing photochemistry of the
578 troposphere. Tellus B, 43(4), 136-151, 1991.
579 Czader, B. H., Rappenglück, B., Percell, P., Byun, D. W., Ngan, F., Kim, S.:
580 Modeling nitrous acid and its impact on ozone and hydroxyl radical during the
581 Texas Air Quality Study 2006. Atmospheric Chemistry and Physics, 12(15),
582 6939-6951, 2012.
583 Dentener, F. J., Crutzen, P. J.: Reaction of N_2O_5 on tropospheric aerosols: Impact on
584 the global distributions of NO_x, O_3, and OH. Journal of Geophysical Research:
585 Atmospheres (1984–2012), 98(D4), 7149-7163, 1993.
586 Elshorbany, Y. F., Kurtenbach, R., Wiesen, P., Lissi, E., Rubio, M., Villena, G.,
587 Gramsch, E., Rickard, A. R., Pilling, M. J., Kleffmann, J.: Oxidation capacity
588 of the city air of Santiago, Chile. Atmospheric Chemistry and Physics, 9(6),
589 2257-2273, 2009.
590 Emmons, L. K., Walters, S., Hess, P. G., Lamarque, J. F., Pfister, G. G., Fillmore, D.,
591 Granier, C., Guenther, A., Kinnison, D., Laepple, T., Orlando, J., Tie, X.,
592 Tyndall, G., Wiedinmyer, C., Baughcum, S. L., Kloster, S.: Description and
593 evaluation of the Model for Ozone and Related chemical Tracers, version 4
594 (MOZART-4). Geoscientific Model Development, 3(1), 43-67, 2010.

595 Fast, J. D., Gustafson, W. I., Easter, R. C., Zaveri, R. A., Barnard, J. C., Chapman, E.
596 G., Grell, G. A., and Peckham, S. E.: Evolution of ozone, particulates, and
597 aerosol direct radiative forcing in the vicinity of Houston using a fully coupled
598 meteorology chemistry aerosol model, J. Geophys. Res. –Atmos., 111(D21), doi:
599 10.1029/2005JD006721, 2006.
600 Finlayson-Pitts, B. J., Wingen, L. M., Sumner, A. L., Syomin, D., Ramazan, K. A.:
601 The heterogeneous hydrolysis of NO_2 in laboratory systems and in outdoor and
602 indoor atmospheres: An integrated mechanism.Physical Chemistry Chemical
603 Physics, 5(2), 223-242, 2003.
604 Fried, A., McKeen, S., Sewell, S., Harder, J., Henry, B., Goldan, P., Kuster, W.,
605 William, E., Baumann, K., Shett, R., Cantrell, C.: Photochemistry of
606 formaldehyde during the 1993 Tropospheric OH Photochemistry
607 Experiment. Journal of Geophysical Research: Atmospheres
608 (1984–2012), 102(D5), 6283-6296, 1997.
609 George, C., Strekowski, R. S., Kleffmann, J., Stemmler, K., Ammann, M.:
610 Photoenhanced uptake of gaseous NO_2 on solid organic compounds: a
611 photochemical source of HONO?. Faraday discussions, 130, 195-210, 2005.
612 Gonçalves, M., Dabdub, D., Chang, W. L., Jorba, O., Baldasano, J. M.: Impact of
613 HONO sources on the performance of mesoscale air quality models.
614 Atmospheric Environment, 54, 168-176, 2012.
615 Grell, G. A., Peckham, S. E., Schmitz, R., McKeen, S. A., Frost, G., Skamarock, W.
616 C., Eder, B.: Fully coupled “online” chemistry within the WRF model.

617 Atmospheric Environment, 39(37), 6957-6975, 2005.
618 Hens, K., Novelli, A., Martinez, M., Auld, J., Axinte, R., Bohn, B., Fischer, H.,
619 Keronen, P., Kubistin, D., Nölscher, A. C., Oswald, R., Paasonen, P., Petäjä, T.,
620 Regelin, E., Sander, R., Sinha, V., Sipilä, M., Taraborrelli, D., Tatum Ernest, C.,
621 Williams, J., Lelieveld, J., Harder, H.: Observation and modeling of HO_x
622 radicals in a boreal forest. Atmospheric Chemistry and Physics, 14, 8723–8747,
623 2014.
624 Jacob, D. J.: Heterogeneous chemistry and tropospheric ozone. Atmospheric
625 Environment, 34(12), 2131-2159, 2000.
626 Kanaya, Y., Pochanart, P., Liu, Y., Li, J., Tanimoto, H., Kato, S., Suthawaree. J.,
627 Inomata, S., Taketani, F., Okuzawa, K., Kawamura, K., Akimoto, H., Wang, Z.
628 F.: Rates and regimes of photochemical ozone production over Central East
629 China in June 2006: a box model analysis using comprehensive measurements
630 of ozone precursors. Atmospheric Chemistry and Physics, 9, 7711–7723, 2009.
631 Kerbrat, M., Legrand, M., Preunkert, S., Gallée, H., and Kleffmann, J.: Nitrous acid
632 at Concordia (inland site) and Dumont d'Urville (coastal site), East Antarctica,
633 J. Geophys. Res. –Atmos., 117(D8), doi: 10.1029/2011JD017149, 2012.
634 Kleffmann, J., Gavriloaiei, T., Hofzumahaus, A., Holland, F., Koppmann, R., Rupp,
635 L., Schlosser, E., Siese, M., Wahner, A.: Daytime formation of nitrous acid: A
636 major source of OH radicals in a forest. Geophysical Research Letters, 32(5),
637 doi: 10.1029/2005GL022524, 2005.
638 Li, G., Lei, W., Zavala, M., Volkamer, R., Dusanter, S., Stevens, P., Molina1, L. T.:

639 Impacts of HONO sources on the photochemistry in Mexico City during the
640 MCMA-2006/MILAGO Campaign. Atmospheric Chemistry and Physics, 10,
641 6551–6567, 2010.
642 Li, L., Chen, C. H., Huang, C., Huang, H. Y., Zhang, G. F., Wang, Y. J., Wang,
643 H. L., Lou, S. R., Qiao, L. P., Zhou, M., Chen, M. H., Chen, Y. R., Fu,
644 J. S., Streets, D. G., Jang, C. J.: Process analysis of regional ozone formation
645 over the Yangtze River Delta, China using the Community Multi-scale Air
646 Quality modeling system. Atmospheric Chemistry and Physics, 12,
647 10971-10987, 2012.
648 Li, S., Matthews, J., Sinha, A.: Atmospheric hydroxyl radical production from
649 electronically excited NO_2 and H_2O. Science, 319, 1657–1660, 2008.
650 Li, X., Brauers, T., Häseler, R., Bohn, B., Fuchs, H., Hofzumahaus, A., Holland, F.,
651 Lou, S., Lu, K. D., Rohrer, F., Hu, M., Zeng, L. M., Zhang, Y. H., Garland, R.
652 M., Su, H., Nowak, A., Wiedensohler, A., Takegawa, N., Shao, M., Wahner, A.:
653 Exploring the atmospheric chemistry of nitrous acid (HONO) at a rural site in
654 Southern China. Atmospheric Chemistry and Physics, 12(3), 1497-1513, 2012.
655 Li, X., Rohrer, F., Hofzumahaus, A., Brauers, T., Häseler, R., Bohn, B., Broch, S.,
656 Fuchs, H., Gomm, S., Holland, F., Jäger, J., Kaiser, J., Keutsch, F. N., Lohse, I.,
657 Lu K., Tillmann, R., Wegener, R., Wolfe, G. M., Mentel, T. F., Kiendler-Scharr,
658 A., Wahner A.: Missing gas-phase source of HONO inferred from Zeppelin
659 measurements in the troposphere. Science, 344, 292-296, 2014.
660 Li, X., Rohrer, F., Hofzumahaus, A., Brauers, T., Häseler, R., Bohn, B., Broch, S.,

661 Fuchs, H., Gomm, S., Holland, F., Jäger, J., Kaiser, J., Keutsch, F. N., Lohse, I.,
662 Lu K., Tillmann, R., Wegener, R., Wolfe, G. M., Mentel, T. F., Kiendler-Scharr,
663 A., Wahner A.: Response to comment on "Missing gas-phase source of HONO
664 inferred from Zeppelin measurements in the troposphere". Science, 348,
665 1326-1326, 2015.
666 Li, Y., An, J., Min, M., Zhang, W., Wang, F., Xie, P.: Impacts of HONO sources on
667 the air quality in Beijing, Tianjin and Hebei Province of China. Atmospheric
668 Environment, 45(27), 4735-4744, 2011.
669 Liu, Z., Wang, Y., Gu, D., Zhao, C., Huey, L. G., Sticke, R., Liao, J., Shao, M., Zhu,
670 T., Zeng, L., Amoroso, A., Costabile, F., Chang, C.-C., Liu, S.-C.: Summertime
671 photochemistry during CARE Beijing-2007: RO_x budgets and O_3 formation.
672 Atmospheric Chemistry and Physics, 12, 7737–7752, 2012.
673 Lu, K. D., Rohrer, F., Holland, F., Fuchs, H., Bohn, B., Brauers, T., Chang, C. C.,
674 Haseler, R., Hu, M., Kita, K., Kondo, Y., Li, X., Lou, S. R., Nehr, S., Shao, M.,
675 Zeng, L. M., Wahner, A., Zhang, Y. H., Hofzumahaus, A.: Observation and
676 modelling of OH and HO_2 concentrations in the Pearl River Delta 2006: a
677 missing OH source in a VOC rich atmosphere. Atmospheric Chemistry and
678 Physics, 12(3), 1541-1569, 2012.
679 Ma, J. Z., Wang, W., Chen, Y., Liu, H. J., Yan, P., Ding, G. A., Wang, M. L., Sun, J.,
680 Lelieveld, J.: The IPAC-NC field campaign: a pollution and oxidization pool in
681 the lower atmosphere over Huabei, China. Atmospheric Chemistry and Physics,
682 12, 3883–3908, 2012.

683 Michoud, V., Colomb, A., Borbon, A., Miet, K., Beekmann, M., Camredon, M.,
684 Aumont, B., Perrier, S., Zapf, P., Siour, G., Ait-Helal, W., Afif, C., Kukui, A.,
685 Furger, M., Dupont, J. C., Haeffelin, M., Doussin, J. F.: Study of the unknown
686 HONO daytime source at a European suburban site during the MEGAPOLI
687 summer and winter field campaigns. Atmospheric Chemistry and Physics, 14(6),
688 2805-2822, 2014.
689 Monge, M. E., D'Anna, B., Mazri, L., Giroir-Fendler, A., Ammann, M., Donaldson,
690 D. J., George, C.: Light changes the atmospheric reactivity of soot. Proceedings
691 of the National Academy of Sciences, 107(15), 6605-6609, 2010.
692 Oswald, R., Behrendt, T., Ermel, M., Wu, D., Su, H., Cheng, Y., Breuninger, C.,
693 Moravek, A., Mougin, E., Delon, C., Loubet, B., Pommerening-Röser, A.,
694 Sörgel, M., Pöschl, U., Hoffmann, T., Andreae, M.O., Meixner, F.X., Trebs, I.:
695 HONO emissions from soil bacteria as a major source of atmospheric reactive
696 nitrogen. Science 341, 1233-1235, 2013.
697 Paulson, S. E., Sen, A. D., Liu, P., Fenske, J. D., Fox, M. J.: Evidence for formation
698 of OH radicals from the reaction of O_3 with alkenes in the gas
699 phase. Geophysical research letters, 24(24), 3193-3196, 1997.
700 Platt, U., Perner, D., Harris, G. W., Winer, A. M., Pitts, J. N.: Observations of
701 nitrous acid in an urban atmosphere by differential optical absorption.
702 Nature 285, 312-314 (29 May 1980); doi: 10.1038/285312a0, 1980.
703 Qin, M., Xie, P. H., Liu, W. Q., Li, A., Dou, K., Fang, W., Liu, J., Zhang, W. J.:
704 Observation of atmospheric nitrous acid with DOAS in Beijing, China. Journal

of Environmental Sciences, 18(1), 69-75, 2006.

Qin, M., Xie, P., Su, H., Gu, J., Peng, F., Li, S., Zengb, L., Liua, J., Liua W., Zhang, Y.: An observational study of the HONO–NO_2 coupling at an urban site in Guangzhou City, South China. Atmospheric Environment, 43(36), 5731-5742, 2009.

Ren, X., Gao, H., Zhou, X., Crounse, J. D., Wennberg, P. O., Browne, E. C., LaFranchi, B. W., Cohen, R. C., McKay, M., Goldstein, A. H., Mao, J.: Measurement of atmospheric nitrous acid at Bodgett Forest during BEARPEX2007. Atmospheric Chemistry and Physics, 10(13), 6283-6294, 2010.

Ren, X., Harder, H., Martinez, M., Lesher, R. L., Oliger, A., Simpas, J. B., Brunea, W. H., Schwab, J. J., Demerjian, K. L., He, Y., Zhou, X., Gao, H.: OH and HO_2 Chemistry in the urban atmosphere of New York City. Atmospheric Environment, 37(26), 3639-3651, 2003.

Ren, X., Sanders, J. E., Rajendran, A., Weber, R. J., Goldstein, A.H., Pusede, S. E., Browne, E. C., Min, K.-E., and Cohen, R.C.: A relaxed eddy accumulation system for measuring vertical fluxes of nitrous acid, Atmos. Meas. Tech., 4, 2093–2103, doi:10.5194/amt-4-2093-2011, 2011.

Rohrer, F., Bohn, B., Brauers, T., Brüning, D., Johnen, F. J., Wahner, A., Kleffmann, J.: Characterisation of the photolytic HONO-source in the atmosphere simulation chamber SAPHIR. Atmospheric Chemistry and Physics, 5(8), 2189-2201, 2005.

727 Sörgel, M., Regelin, E., Bozem, H., Diesch, J. M., Drewnick, F., Fischer, H., Harder,
728 H., Held, A., Hosaynali-Beygi, Z., Martinez, M., Zetzsch, C.: Quantification of
729 the unknown HONO daytime source and its relation to NO_2. Atmospheric
730 Chemistry and Physics, 11(20), 10433-10447, 2011.
731 Sarwar, G., Roselle, S. J., Mathur, R., Appel, W., Dennis, R. L., Vogel, B.: A
732 comparison of CMAQ HONO predictions with observations from the Northeast
733 Oxidant and Particle Study. Atmospheric Environment, 42(23), 5760-5770,
734 2008.
735 Spataro, F., Ianniello, A., Esposito, G., Allegrini, I., Zhu, T., Hu, M.: Occurrence of
736 atmospheric nitrous acid in the urban area of Beijing (China).Science of the
737 Total Environment, 447, 210-224, 2013.
738 Stemmler, K., Ammann, M., Donders, C., Kleffmann, J., George, C.:
739 Photosensitized reduction of nitrogen dioxide on humic acid as a source of
740 nitrous acid. Nature, 440(7081), 195-198, 2006.
741 Stemmler, K., Ndour, M., Elshorbany, Y., Kleffmann, J., D'anna, B., George,
742 C., Bohn, B., Ammann, M.: Light induced conversion of nitrogen dioxide into
743 nitrous acid on submicron humic acid aerosol. Atmospheric Chemistry and
744 Physics, 7(16), 4237-4248, 2007.
745 Stone, D., Whalley, L. K., Heard, D. E.: Tropospheric OH and HO_2 radicals: field
746 measurements and model comparisons. Chemical Society Reviews, 41,
747 6348-6404, 2012.

748 Su, H., Cheng, Y., Oswald, R., Behrendt, T., Trebs, I., Meixner, F. X., Andreae, M.
749 O., Cheng, P., Zhang, Y., Pöschl, U.: Soil nitrite as a source of atmospheric
750 HONO and OH radicals. Science, 333(6049), 1616-1618, 2011.
751 Su, H., Cheng, Y. F., Shao, M., Gao, D. F., Yu, Z. Y., Zeng, L. M., Slanina, J., Zhang,
752 Y. H., and Wiedensohler, A.: Nitrous acid (HONO) and its daytime sources at a
753 rural site during the 2004 PRIDE-PRD experiment in China, J. Geophys. Res.
754 –Atmos., 113(D14), doi: 10.1029/2007JD009060, 2008.
755 Tang, Y., An, J., Li, Y., Wang, F.: Uncertainty in the uptake coefficient for HONO
756 formation on soot and its impacts on concentrations of major chemical
757 components in the Beijing–Tianjin–Hebei region. Atmospheric Environment,
758 84, 163-171, 2014.
759 VandenBoer, T. C., Brown, S. S., Murphy, J. G., Keene, W. C., Young, C. J.,
760 Pszenny, A. A. P., Kim, S., Warneke, C., de Gouw, J. A., Maben, J. R., Wagner,
761 N. L., Riedel, T. P., Thornton, J. A., Wolfe, D. E., Dubé, W. P., Öztürk, F.,
762 Brock, C. A., Grossberg, N., Lefer, B., Lerner, B. Middlebrook, A. M., Roberts,
763 J. M.: Understanding the role of the ground surface in HONO vertical structure:
764 High resolution vertical profiles during NACHTT-11. Journal of Geophysical
765 Research: Atmospheres, 118, 10,155–10,171, doi:10.1002/jgrd.50721, 2013.
766 Villena, G., Wiesen, P., Cantrell, C. A., Flocke, F., Fried, A., Hall, S. R., Hornbrook,
767 R. S., Knapp, D., Kosciuch, E., Mauldin, R. L., McGrath, J. A., Montzka, D.,
768 Richter, D., Ullmann, K., Walega, J., Weibring, P., Weinheimer, A., Staebler, R.
769 M., Liao, J., Huey, L. G., and Kleffmann, J.: Nitrous acid (HONO) during polar

770 spring in Barrow, Alaska: a net source of OH radicals?, J. Geophys. Res.
771 –Atmos., 116(D14), doi: 10.1029/2011JD016643, 2011.
772 Wang, F., An, J., Li, Y., Tang, Y., Lin, J., Qu, Y., Cheng, Y., Zhang, B., Zhai, J.:
773 Impacts of Uncertainty in AVOC Emissions on the Summer RO_x Budget and
774 Ozone Production Rate in the Three Most Rapidly-Developing Economic
775 Growth Regions of China. Advances in Atmospheric Sciences, 31, 1331–1342,
776 2014.
777 Wang, X., Zhang, Y., Hu, Y., Zhou, W., Lu, K., Zhong, L., Zeng, L., Shao, M., Hu,
778 M., Russell, A. G.: Process analysis and sensitivity study of regional ozone
779 formation over the Pearl River Delta, China, during the PRIDE-PRD2004
780 campaign using the Community Multiscale Air Quality modeling
781 system. Atmospheric Chemistry and Physics, 10(9), 4423-4437, 2010.
782 Wong, K. W., Oh, H. J., Lefer, B. L., Rappenglück, B., Stutz, J.: Vertical profiles of
783 nitrous acid in the nocturnal urban atmosphere of Houston, TX. Atmospheric
784 Chemistry and Physics, 11(8), 3595-3609, 2011.
785 Wong, K. W., Tsai, C., Lefer, B., Grossberg, N., Stutz, J.: Modeling of daytime
786 HONO vertical gradients during SHARP 2009. Atmospheric Chemistry and
787 Physics, 13(7), 3587-3601, 2013.
788 Wong, K. W., Tsai, C., Lefer, B., Haman, C., Grossberg, N., Brune, W. H., Ren,
789 X., Luke, W., Stutz, J.: Daytime HONO vertical gradients during SHARP 2009
790 in Houston, TX. Atmospheric Chemistry and Physics, 12(2), 635-652, 2012.
791 Wu, J., Xu, Z., Xue, L., Wang, T.: Daytime nitrous acid at a polluted suburban site

792 in Hong Kong: Indication of heterogeneous production on aerosol. Proceedings
793 of 12th international conference on atmospheric sciences and applications to air
794 quality, Seoul, Korea, June 3-5, 2013, p. 52, 2013.
795 Ye, C., Zhou, X., Pu, D., Stutz, J., Festa, J., Spolaor, M., Cantrell, C., Mauldin, R. L.,
796 Weinheimer, A., Haggerty, J.: Comment on "Missing gas-phase source of
797 HONO inferred from Zeppelin measurements in the troposphere". Science, 348,
798 1326-d, 2015.
799 Zaveri, R. A., Peters, L. K.: A new lumped structure photochemical mechanism for
800 large‐scale applications. Journal of Geophysical Research: Atmospheres
801 (1984–2012), 104(D23), 30387-30415, 1999.
802 Zaveri, R. A., Easter, R. C., Fast, J. D., and Peters, L. K.: Model for simulating
803 aerosol interactions and chemistry (MOSAIC), J. Geophys. Res. –Atmos.,
804 113(D13), doi: 10.1029/2007JD008782, 2008.
805 Zhang, B., Tao, F.: Direct homogeneous nucleation of NO_2, H_2O, and NH_3 for the
806 production of ammonium nitrate particles and HONO gas. Chemical Physics
807 Letters, 489, 4-6, 143, 2010.
808 Zhang, H., Li, J., Ying, Q., Yu, J. Z., Wu, D., Cheng, Y., Kebin Hed, Jiang, J.:
809 Source apportionment of $PM_{2.5}$ nitrate and sulfate in China using a
810 source-oriented chemical transport model. Atmospheric Environment, 62,
811 228-242, 2012.
812 Zhang, N., Zhou, X., Bertman, S., Tang, D., Alaghmand, M., Shepson, P. B., Carroll,
813 M. A.: Measurements of ambient HONO concentrations and vertical HONO

814 flux above a northern Michigan forest canopy. Atmospheric Chemistry and
815 Physics, 12(17), 8285-8296, 2012.
816 Zhang, Q., Streets, D. G., Carmichael, G. R., He, K., Huo, H., Kannari, A., Klimont,
817 Z., Park, I., Reddy, S., Fu, J. S., Chen, D., Duan, L., Lei, Y., Wang, L., Yao, Z.:
818 Asian emissions in 2006 for the NASA INTEX-B mission. Atmospheric
819 Chemistry and Physics, 9, 5131-5153, 2009.
820 Zhou, X., Civerolo, K., Dai, H., Huang, G., Schwab, J., and Demerjian, K:
821 Summertime nitrous acid chemistry in the atmospheric boundary layer at a rural
822 site in New York State, J. Geophys. Res. –Atmos., 107(D21), ACH13-1 –
823 ACH13-11, doi: 10.1029/2001JD001539, 2002a.
824 Zhou, X., Gao, H., He, Y., Huang, G., Bertman, S. B., Civerolo, K., and Schwab, J.:
825 Nitric acid photolysis on surfaces in low-NO_x environments: significant
826 atmospheric implications, Geophys. Res. Lett., 30(23), doi:
827 10.1029/2003GL018620, 2003.
828 Zhou, X., He, Y., Huang, G., Thornberry, T. D., Carroll, M. A., and Bertman, S. B.:
829 Photochemical production of nitrous acid on glass sample manifold surface,
830 Geophys. Res. Lett., 29, 26-1 – 26-4, doi: 10.1029/2002GL015080, 2002b.
831 Zhou, X., Zhang, N., TerAvest, M., Tang, D., Hou, J., Bertman, S., Alaghmand, M.,
832 Shepson, P. B. Carroll, M. A. Griffith, S., Dusanter, S., Stevens, P. S.: Nitric
833 acid photolysis on forest canopy surface as a source for tropospheric nitrous
834 acid. Nature Geoscience, 4(7), 440-443, 2011.

835 Table 1. Model performance statistics for O_3 and NO_2 in Beijing in August 2007 and Guangzhou in July 2006.

Species	Case	MB (ppb)	ME (ppb)	RMSE (ppb)	NMB (%)	NME (%)	IOA
O_3	R_p	−0.65	19.40	25.44	−2.20	66.10	0.80
	R	−6.69	17.21	25.24	−22.80	58.70	0.79
NO_2	R_p	−9.50	17.31	21.40	−29.10	53.00	0.51
	R	−4.40	13.75	17.61	−13.50	42.10	0.57

836 MB: mean bias; ME: mean error; RMSE: root-mean-square error; NMB: normalized mean bias; NME: normalized mean error; IOA: index of
837 agreement.
838
839
840
841
842
843
844
845

Table 2. Model performance statistics for daytime (06:00–18:00 LST) and nighttime (19:00–05:00 LST) HONO in Beijing in August 2007 and Guangzhou in July 2006.

Species	Case	MB (10^6 molec cm^{-3})	ME (10^6 molec cm^{-3})	RMSE (10^6 molec cm^{-3})	NMB (%)	NME (%)	IOA	CC
$HONO_{daytime}$ (Beijing)	R_p	−0.54	0.98	1.41	−24.30	44.50	0.73	0.57
	R_{wop}	−1.37	1.41	1.83	−62.00	64.10	0.64	0.63
	R	−2.07	2.07	2.58	−93.80	93.80	0.46	0.31
$HONO_{nighttime}$ (Beijing)	R_p	−0.73	0.84	1.09	−42.20	49.10	0.77	0.74
	R_{wop}	−0.82	0.91	1.16	−47.90	53.20	0.75	0.75
	R	−1.68	1.68	2.06	−97.90	97.90	0.46	0.76
$HONO_{daytime}$ (Guangzhou)	R_p	−0.38	0.43	0.58	−61.20	69.60	0.58	0.56
	R_{wop}	−0.48	0.49	0.65	−76.50	77.70	0.55	0.56
	R	−0.60	0.60	0.80	−95.60	96.20	0.43	-0.30
$HONO_{nighttime}$ (Guangzhou)	R_p	−0.42	0.75	1.05	−32.90	58.50	0.66	0.43
	R_{wop}	−0.49	0.83	1.15	−38.40	64.30	0.63	0.38
	R	−1.25	1.25	1.59	−97.20	97.20	0.45	-0.01

CC: correlation coefficient.

Table 3. Model performance statistics for OH and HO_2 in Guangzhou in July 2006.

Species	Case	MB (10^6 molec cm^{-3})	ME (10^6 molec cm^{-3})	RMSE (10^6 molec cm^{-3})	NMB (%)	NME (%)	IOA	CC
OH	R_p	−1.35	4.37	6.22	−17.60	57.00	0.84	0.75
	R_{wop}	−3.00	4.58	6.25	−112.20	126.50	0.81	0.72
	R	−3.36	4.85	6.55	−123.00	136.60	0.79	0.70
HO_2	R_p	−3.80	3.81	5.59	−78.50	78.60	0.61	0.66
	R_{wop}	−4.19	4.20	6.14	−86.60	86.70	0.54	0.59
	R	−4.22	4.23	6.16	−87.20	87.30	0.54	0.57

857 Table 4. Daytime (06:00–18:00 LST) average OH budgets in Beijing/Shanghai/Guangzhou in August 2007.
858

Reaction	Case R		Case R_{wop}		Case R_p	
	Rate (ppb h^{-1})	Contribution (%)	Rate (ppb h^{-1})	Contribution (%)	Rate (ppb h^{-1})	Contribution (%)
OH production						
HO_2+NO	**2.778/0.732/1.748**	**81.73/67.09/71.54**	**3.242/0.760/1.871**	**83.74/68.00/72.02**	**7.101/1.402/2.553**	**73.34/61.95/67.55**
$^*(HONO+hv)_{net}$	**--/--/--**	**--/--/--**	**--/--/0.017**	**--/--/0.66**	**1.855/0.497/0.489**	**19.16/21.98/12.93**
O^1D+H_2O	**0.465/0.307/0.617**	**13.68/28.17/25.27**	**0.479/0.306/0.630**	**12.36/27.38/24.24**	**0.568/0.312/0.651**	**5.86/13.80/17.23**
O_3+OLET/OLEI	0.101/0.024/0.027	2.98/2.16/1.11	0.095/0.023/0.027	2.45/2.08/1.03	0.080/0.021/0.025	0.83/0.91/0. 65
$^*(H_2O_2+hv)_{net}$	0.035/0.023/0.029	1.02/2.07/1.17	0.035/0.023/0.030	0.91/2.03/1.16	0.037/0.022/0.032	0.38/0.97/0.19
HO_2+O_3	0.009/0.001/0.014	0.28/0.07/0.59	0.010/0.001/0.015	0.26/0.06/0.58	0.026/0.001/0.019	0.27/0.05/0.51
$^*(HNO_3+hv)_{net}$	0.005/0.001/0.002	0.15/0.06/0.10	0.005/0.001/0.002	0.13/0.06/0.09	0.007/0.001/0.003	0.07/0.04/0.07
ROOH+hv	0.003/0.004/0.005	0.09/0.36/0.19	0.003/0.004/0.005	0.09/0.38/0.19	0.007/0.007/0.007	0.07/0.29/0.19
O_3+ETH	0.002/<0.001/<0.001	0.05/0.02/0.01	0.002/<0.001/<0.001	0.04/0.02/0.01	0.001/<0.001/<0.001	0.02/0.01/0.01
HO_2+NO_3	<0.001/<0.001/<0.001	<0.01/<0.01/0.01	<0.001/<0.001/<0.001	<0.01/<0.01/<0.01	<0.001/<0.001/<0.001	<0.01/<0.01/<0.01
O_3+ISOP	<0.001/<0.001/<0.001	0.01/<0.01/<0.01	<0.001/<0.001/<0.001	0.01/<0.01/<0.01	<0.001/<0.001/<0.001	<0.01/<0.01/<0.01
Total	3.399/1.091/2.443	100/100/100	3.873/1.118/2.598	100/100/100	9.683/2.263/3.779	100/100/100
OH loss						
OH+NO_2	**1.116/0.474/0.770**	**39.31/46.63/38.33**	**1.225/0.501/0.844**	**38.11/45.86/38.86**	**3.146/1.045/1.424**	**38.08/44.29/40.76**
OH+CO	**0.785/0.203/0.576**	**27.65/19.97/28.67**	**0.932/0.227/0.637**	**29.00/20.78/29.33**	**2.573/0.506/1.001**	**31.14/21.45/28.65**
OH+OLET/OLEI	**0.192/0.054/0.059**	**6.76/5.31/2.94**	**0.264/0.065/0.077**	**8.21/5.95/3.55**	**0.537/0.206/0.095**	**6.50/8.73/2.72**
OH+HCHO	**0.150/0.050/0.146**	**5.28/4.92/7.27**	**0.166/0.053/0.156**	**5.16/4.85/7.18**	**0.544/0.096/0.242**	**6.59/4.07/6.93**
OH+CH_4	0.103/0.057/0.135	3.63/5.61/6.72	0.109/0.059/0.142	3.39/5.40/6.54	0.260/0.115/0.223	3.15/4.87/6.38
OH+ALD2/MGLY/ ANOE	0.092/0.018/0.045	3.24/1.77/2.24	0.109/0.020/0.049	3.39/1.83/2.26	0.323/0.047/0.081	3.91/1.99/2.32

OH+SO_2	0.054/0.030/0.035	1.90/2.95/1.74	0.064/0.034/0.041	1.99/3.11/1.89	0.172/0.116/0.072	2.08/4.92/2.06
OH+XYL	0.052/0.022/0.023	1.83/2.16/1.14	0.066/0.026/0.029	2.05/2.38/1.34	0.141/0.078/0.045	1.71/3.31/1.29
OH+H_2	0.038/0.021/0.050	1.34/2.07/2.49	0.040/0.022/0.052	1.24/2.01/2.39	0.095/0.027/0.075	1.15/1.14/2.15
OH+TOL	0.027/0.007/0.011	0.95/0.69/0.55	0.034/0.008/0.014	1.06/0.73/0.64	0.086/0.025/0.024	1.04/1.06/0.69
OH+HONO	0.003/0.003/0.005	0.11/0.30/0.25	0.006/0.004/0.007	0.19/0.37/0.32	0.069/0.023/0.032	0.84/0.97/0.92
OH+HNO_x	0.005/0.001/0.005	0.18/0.10/0.25	0.005/0.001/0.005	0.16/0.09/0.23	0.015/0.002/0.008	0.18/0.08/0.23
OH+O_3	0.028/0.006/0.035	0.99/0.59/1.70	0.029/0.006/0.036	0.90/0.55/1.66	0.072/0.005/0.046	0.87/0.21/1.32
OH+H_2O_2	0.015/0.008/0.027	0.53/0.79/1.34	0.016/0.008/0.029	0.50/0.73/1.34	0.040/0.010/0.043	0.48/0.42/1.23
OH+ETH/OPEN	0.007/0.002/0.004	0.25/0.20/0.20	0.008/0.002/0.005	0.25/0.18/0.23	0.036/0.009/0.011	0.44/0.38/0.31
OH+CH_3OOH/ROOH	0.010/0.011/0.014	0.35/1.08/0.70	0.011/0.012/0.014	0.34/1.10/0.64	0.022/0.020/0.022	0.27/0.85/0.63
OH+ISOP	0.019/0.004/0.002	0.67/0.39/0.10	0.020/0.004/0.003	0.62/0.37/0.14	0.017/0.007/0.003	0.21/0.30/0.09
OH+PAR	0.005/0.002/0.004	0.18/0.20/0.20	0.007/0.003/0.005	0.22/0.27/0.23	0.015/0.005/0.007	0.18/0.21/0.20
OH+ONIT /ISOPRD	0.028/0.005/0.016	0.99/0.49/0.80	0.030/0.005/0.018	0.93/0.46/0.83	0.077/0.013/0.025	0.93/0.55/0.72
OH+C_2H_6	0.002/0.001/0.002	0.07/0.10/0.10	0.003/0.001/0.002	0.09/0.09/0.09	0.008/0.002/0.004	0.10/0.08/0.11
OH+CH_3OH/ANOL/CRES	0.002/0.001/0.002	0.07/0.10/0.10	0.002/0.001/0.002	0.06/0.09/0.09	0.007/0.002/0.003	0.08/0.08/0.09
OH+HO_2	0.001/<0.001/0.004	0.04/0.05/0.20	0.002/<0.001/0.005	0.06/0.05/0.23	0.006/<0.001/0.008	0.07/0.02/0.23
OH+NO	0.105/0.036/0.039	3.70/3.54/1.94	0.066/0.030/--	2.05/2.75/--	--/--/--	--/--/--
Total	2.839/1.017/2.009	100/100/100	3.214/1.093/2.172	100/100/100	8.261/2.360/3.495	100/100/100

OLET: internal olefin carbons (C=C); OLEI: terminal olefin carbons (C=C); ROOH: higher organic peroxide; ETH: ethene; ISOP: isoprene; ALD2: acetaldehyde; MGLY: methylglyoxal; ANOE: acetone; XYL: xylene; TOL: toluene; HNO_x: HNO_3 + HNO_4; OPEN: aromatic fragments; PAR: paraffin carbon –C–; ONIT: organic nitrate; ISOPRD: lumped intermediate species; ANOL: ethanol; CRES: cresol and higher molar weight phenols.

*The reactions of HONO+hv, H_2O_2+hv and HNO_3+hv are reversible, “net” in the subscript means subtracting the corresponding reverse reactions.

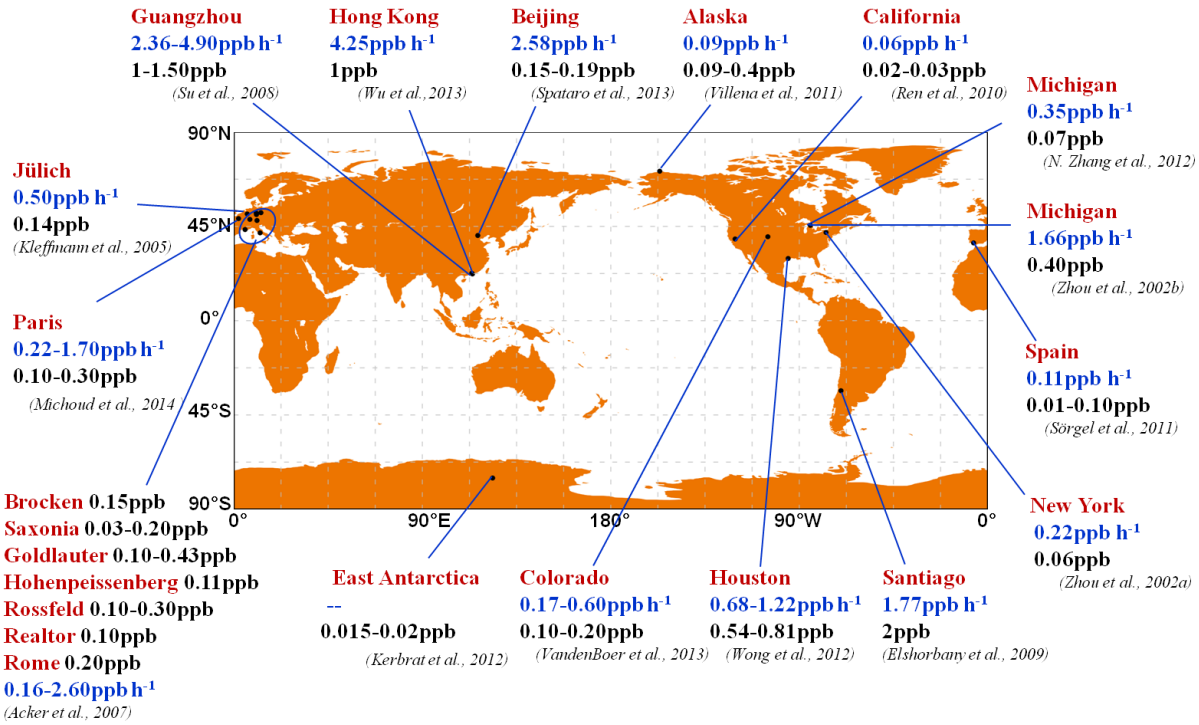

Fig. 1. Summary of observed HONO mixing ratios at noon (black font) and the calculated unknown daytime HONO source (blue font) from field studies.

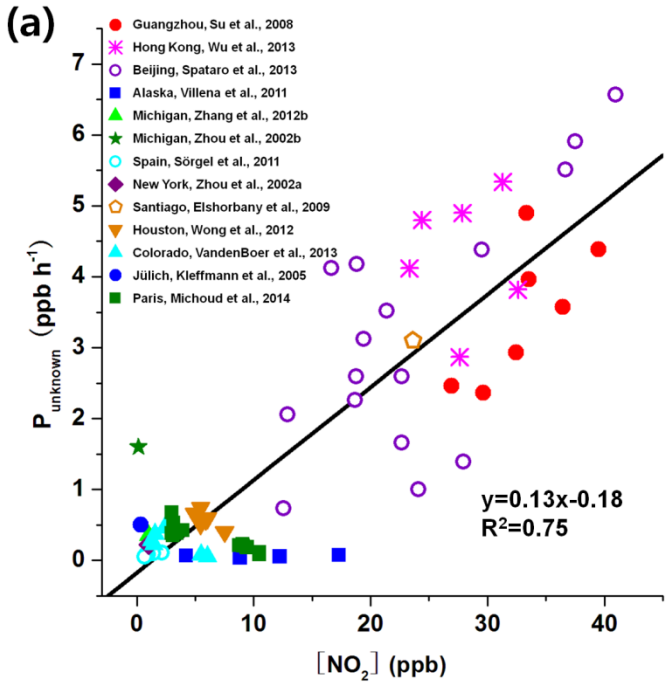

880

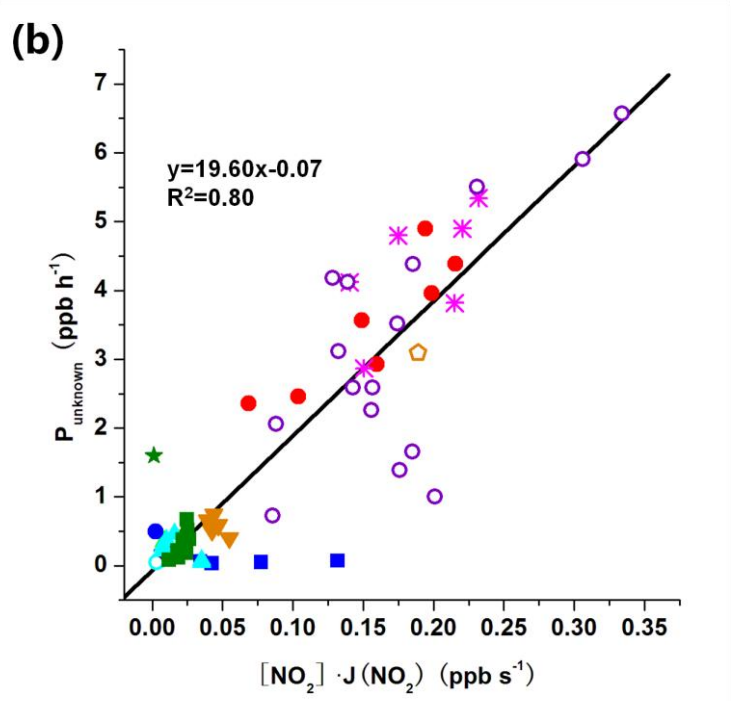

881

882 Fig. 2. Correlation of the unknown daytime HONO source ($P_{unknown}$) (ppb h^{-1}) with (a)

883 [NO_2] (ppb) and (b) [NO_2] × J(NO_2) (ppb s^{-1}), based on the field experiment data

884 shown in Fig. 1.

885

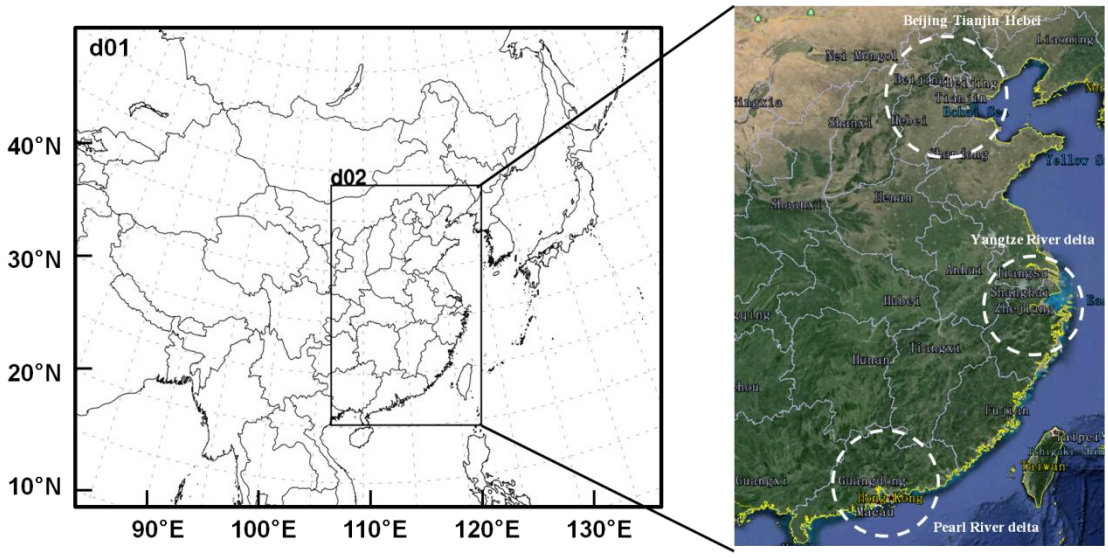

Fig. 3. Model domains used in this study. Domain 2 covers the Beijing–Tianjin–Hebei (BTH), Yangtze River delta (YRD), and Pearl River delta (PRD) regions.

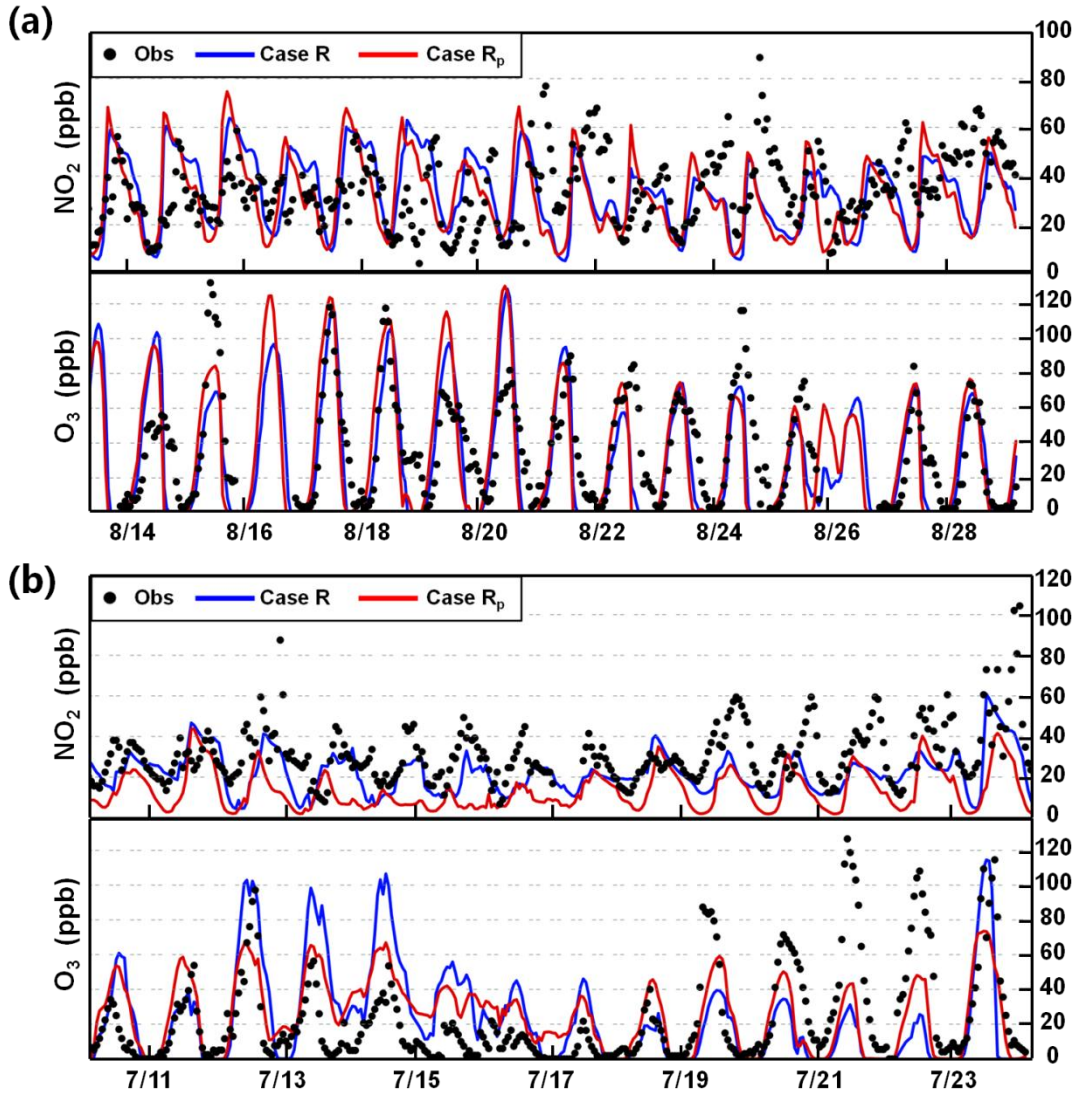

904
905 Fig. 4. Comparison of simulated and observed hourly-mean mixing ratios of NO_2 and
906 O_3 in (a) Beijing on 14–28 August 2007 and (b) Guangzhou on 11–23 July 2006.
907
908
909
910
911
912

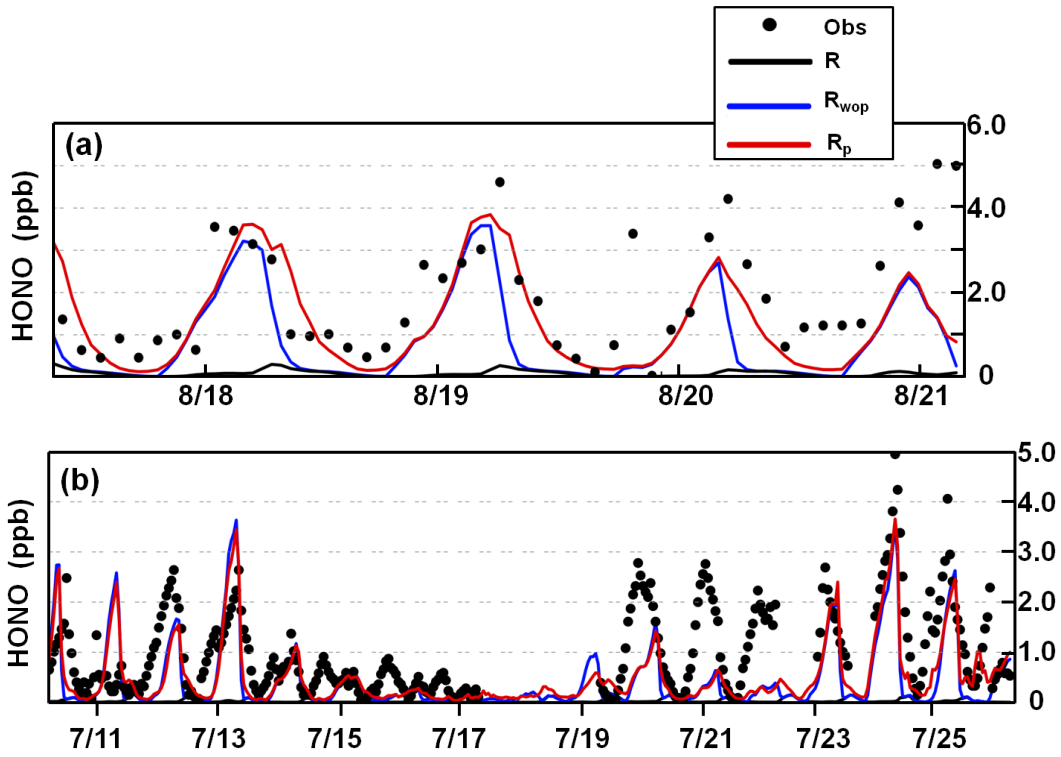

Fig. 5. Comparison of simulated and observed hourly-mean HONO mixing ratios at the Peking University site in (a) Beijing on 17–20 August 2007 (Spataro et al., 2013) and (b) the Backgarden site in Guangzhou on 11–25 July 2006 (X. Li et al., 2012).

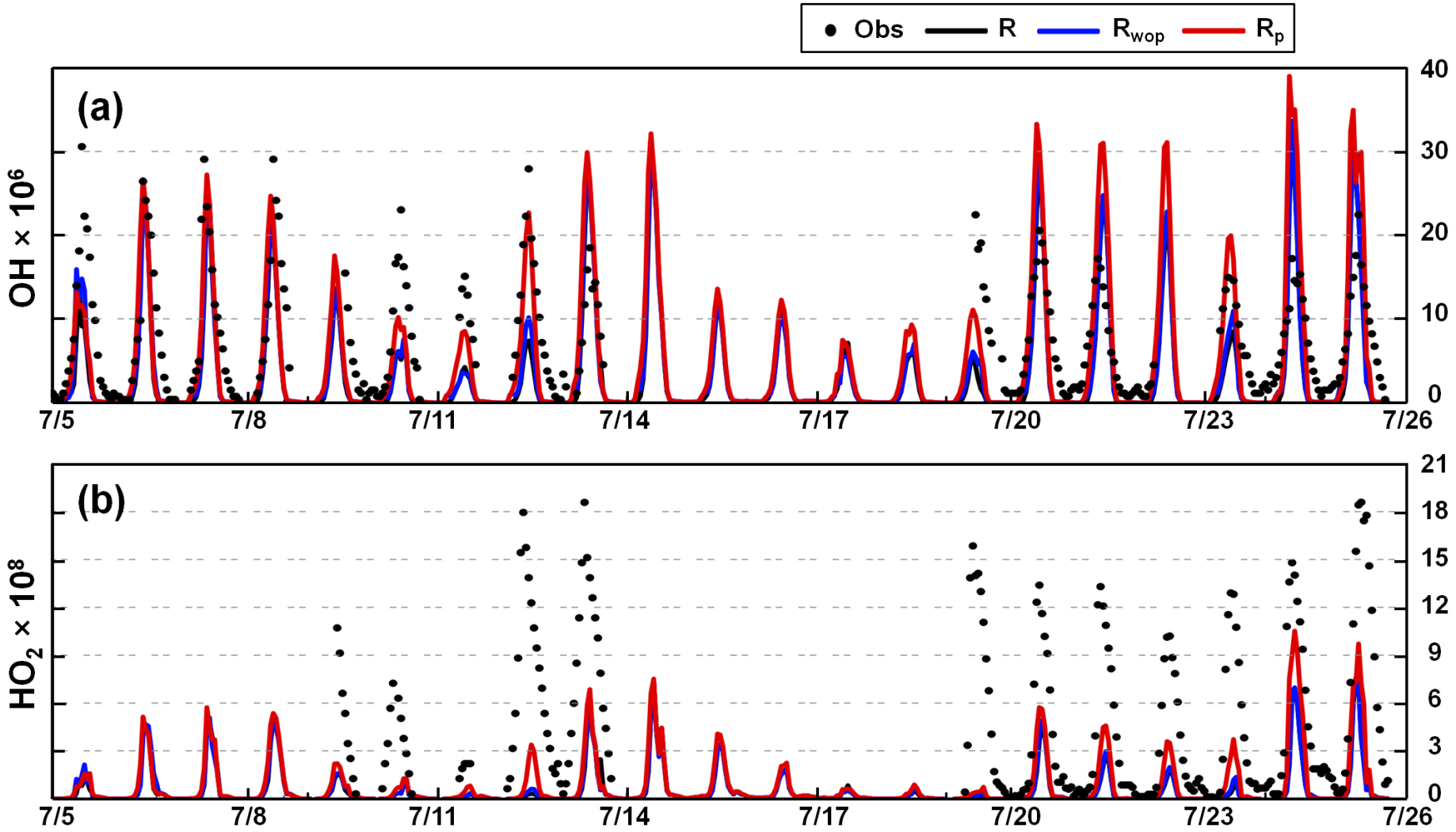

930
931 Fig. 6. Comparison of simulated and observed hourly-mean mixing ratios of OH and HO_2 at the Backgarden site in Guangzhou in July 2006 (Lu

et al., 2012).

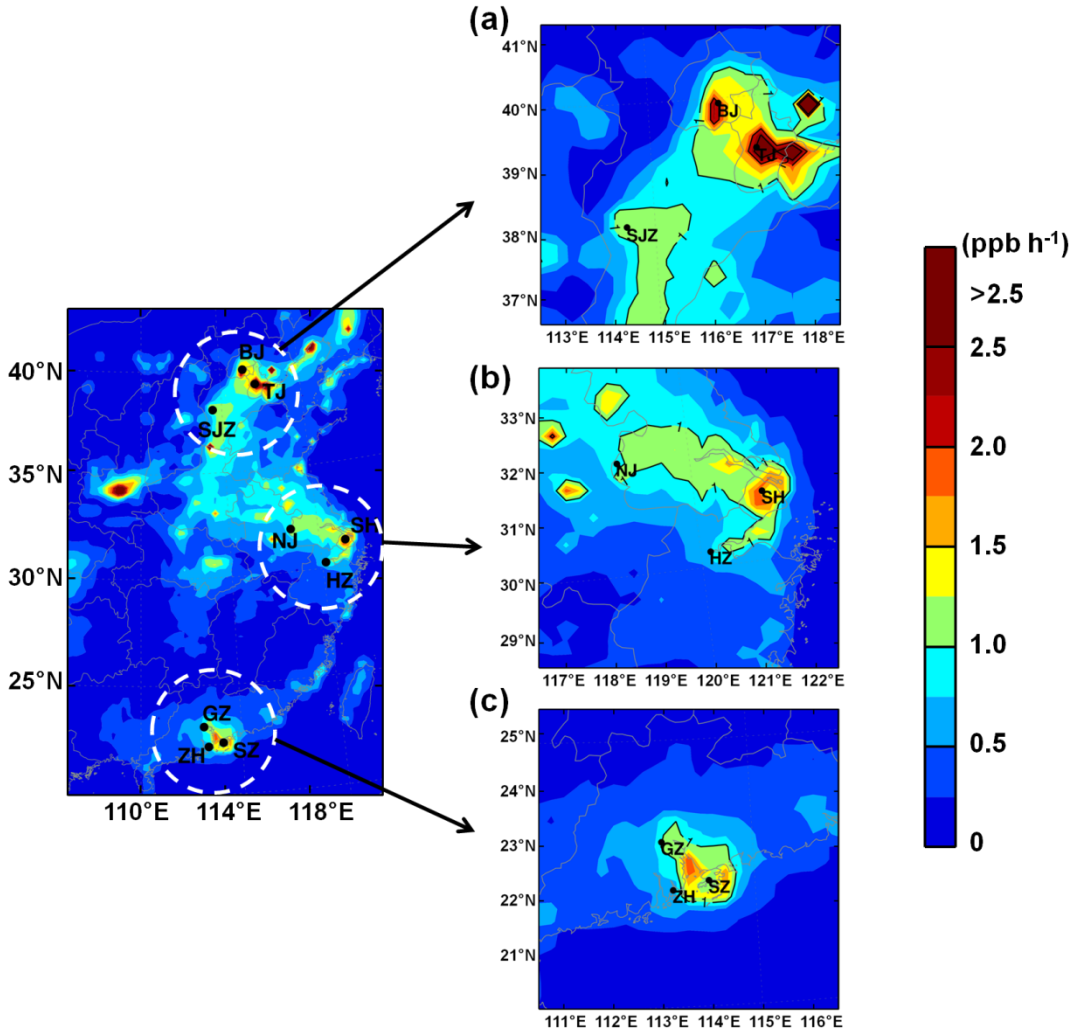

Fig. 7. Simulated unknown daytime HONO source (ppb h^{-1}) in the (a) BTH, (b) YRD, and (c) PRD regions in August 2007 (BJ, Beijing; TJ, Tianjin; SJZ, Shijiazhuang; SH, Shanghai; NJ, Nanjing; HZ, Hangzhou; GZ, Guangzhou; ZH, Zhuhai; SZ, Shenzhen).

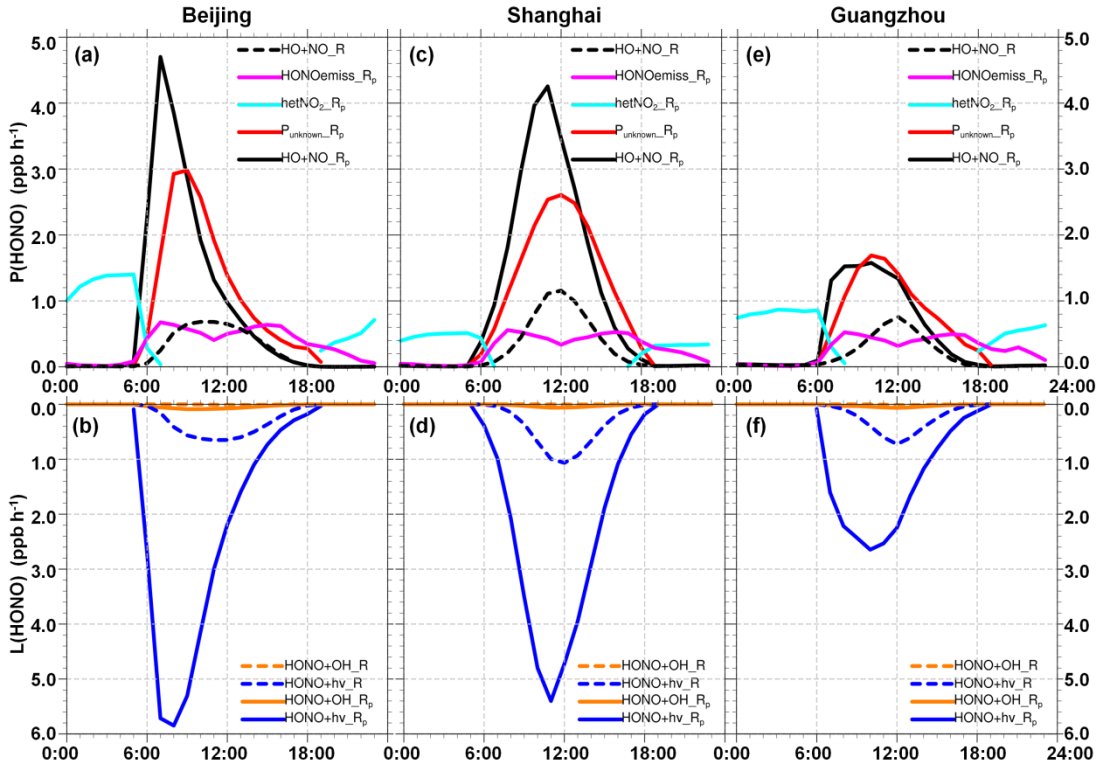

Fig. 8. Production [P(HONO)] and loss [L(HONO)] rates of HONO for cases R (dashed lines) and R_p (solid lines) in (a, b) Beijing, (c, d) Shanghai, and (e, f) Guangzhou in August 2007.

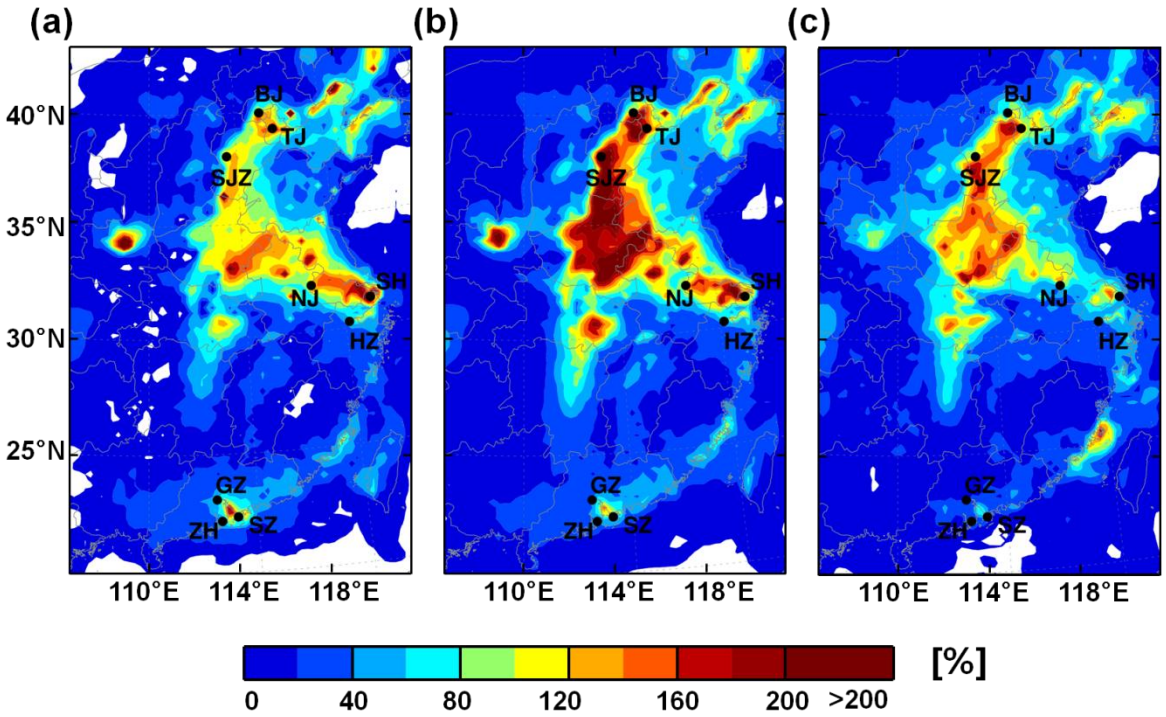

Fig. 9. Daytime (06:00–18:00 LST) percentage enhancements of (a) OH, (b) HO_2, and (c) RO_2 due to the unknown daytime HONO source (case R_p − case R_{wop}) in the coastal regions of China in August 2007.

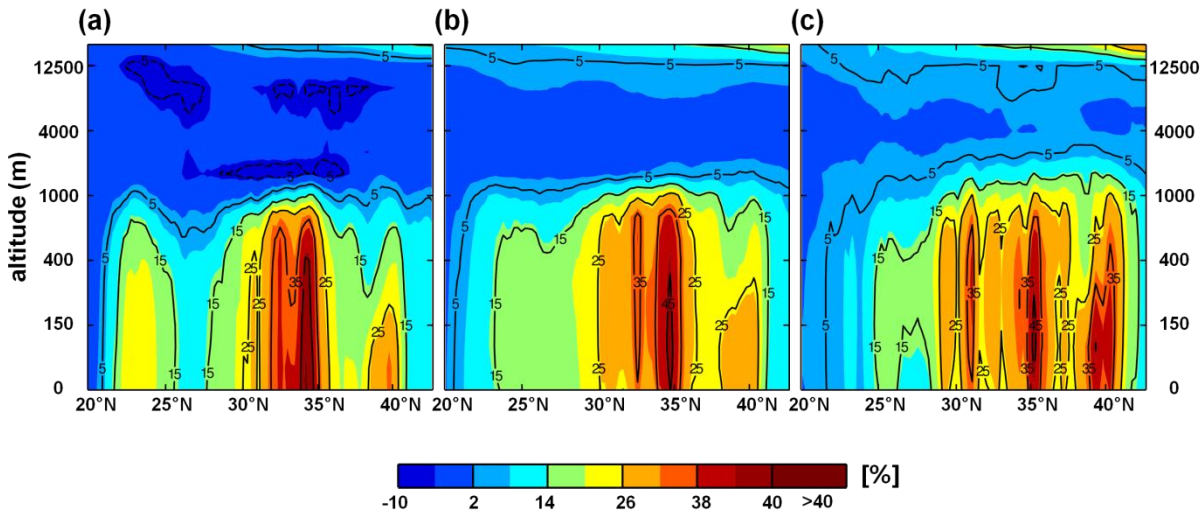

989

990 Fig. 10. Daytime (06:00–18:00 LST) meridional-mean percentage enhancements of (a)

991 OH, (b) HO_2, and (c) RO_2 due to the unknown daytime HONO source (case R_p − case

992 R_{wop}) in the coastal regions of China in August 2007.

993

994

995

996

997

998

999

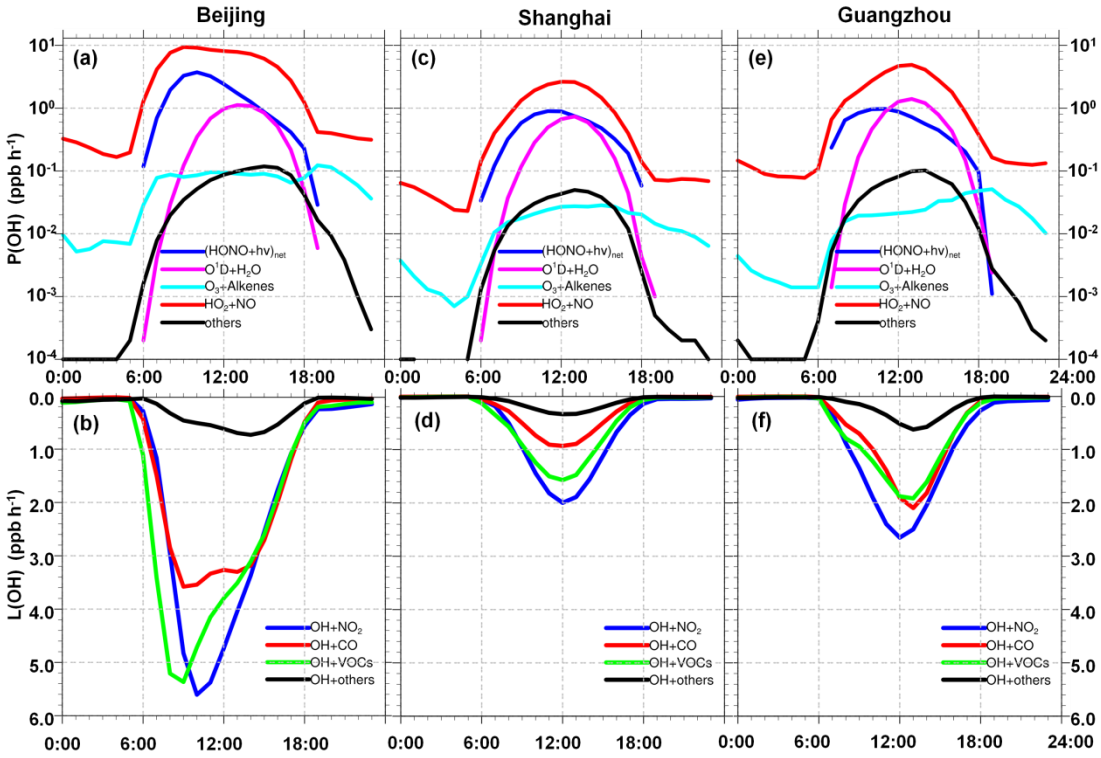

Fig. 11. Averaged production [P(OH)] and loss [L(OH)] rates of OH for case R_p in (a, b) Beijing, (c, d) Shanghai, and (e, f) Guangzhou in August 2007. $(HONO+hv)_{net}$ means the net OH production rate from HONO photolysis (subtracting OH + NO = HONO).

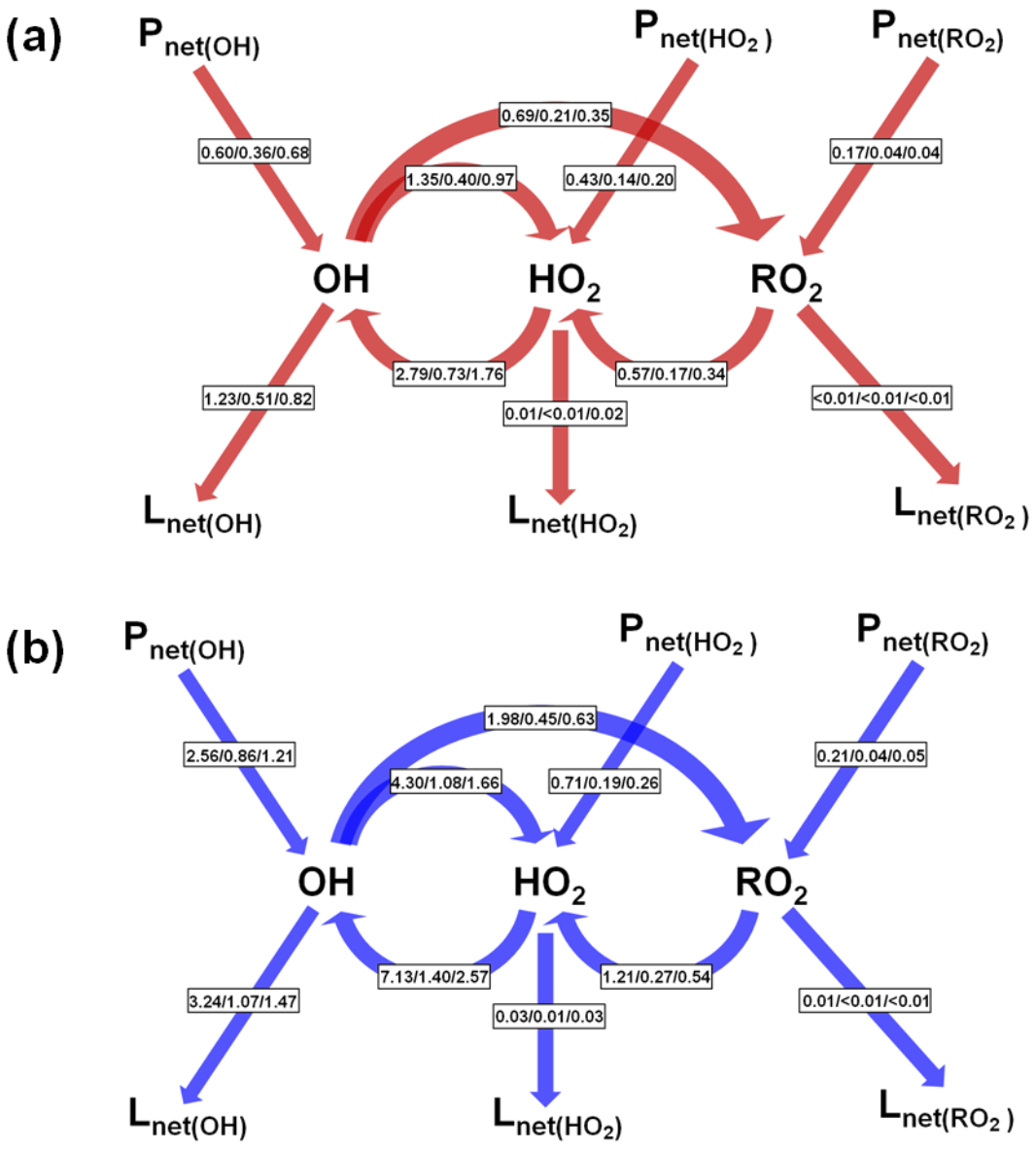

Fig. 12. Daytime (06:00–18:00 LST) average budgets of OH, HO_2 and RO_2 radicals (reaction rates, ppb h^{-1}) for cases (a) R and (b) R_p in Beijing/Shanghai/Guangzhou in August 2007.